Aus dem Institut für Physiologie und Pathophysiologie
Geschäftsführender Direktor: Prof. Dr. Dr. Jürgen Daut

des Fachbereichs Medizin der Philipps-Universität Marburg

Endozytose des Kaliumkanals Kir2.1

Inaugural-Dissertation
Zur Erlangung des Doktorgrades der
Naturwissenschaften (Dr. rer. nat.)

dem Fachbereich Medizin
der Philipps-Universität Marburg
vorgelegt von

Wei Tu

aus Shaanxi, China

Marburg, 2015

Angenommen vom Fachbereich Medizin der Philipps-Universität Marburg

am:

Gedruckt mit Genehmigung des Fachbereichs.

Dekan: Prof. Dr. H. Schäfer

Referent: Prof. Dr. Dr. Jürgen Daut

Korreferent: PD. Dr. Caroline Rolfes

1. Introduction

1.1 Potassium channels

Potassium channels are well known in almost all kinds of cell types in all organisms. They are involved in a multitude of physiological processes of excitable and nonexcitable cells, including regulation of neurotransmitter release, heart rate, insulin secretion, neuronal excitability, epithelial electrolyte transport, smooth muscle contraction, and cell volume regulation (Shieh *et al.*, 2000).

Potassium channels are tetrameric integral membrane proteins forming transmembrane aqueous pores that allow only K+ ions across the cell membrane. The structural element that causes K^+ selectivity is a highly conserved sequence motif (TXXTXGYG). The potassium 'signature sequence' with a GYG (Gly-Tyr-Gly) motif plays an important role to selectively allow K^+ ions to pass through the pore (Heginbotham *et al.*, 1994; Doyle *et al.*, 1998).

Basically, there are four major classes of potassium channels: calcium activated potassium channels, inwardly rectifying potassium channels, two pore domain potassium channels and voltage gated potassium channels.

By comparing primary amino acid sequence of the pore-containing subunit, potassium channel can also be divided into three main groups in mammalians species (Sandoz & Levitz, 2013) (Figure 1.1).

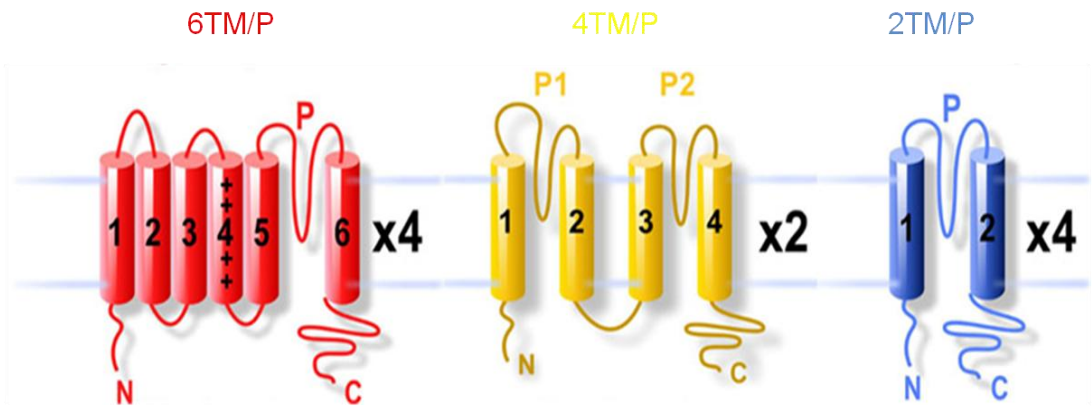

Figure 1.1 Membrane topology of the three potassium channel families. Voltage gated K^+ channel has six transmembrane domains (S1–S6) and one P-domain between S5 and S6. The K2P channels have four transmembrane domains with two pore domain (in the order: TM1, P1, TM2, TM3, P2, TM4). Finally, the inward-rectifier potassium channels have two transmembrane domains (S1 and S2) and one P-domain (Adopted from Sandoz and Levitz, 2013).

(1) 6TM/1P channels: They are composed of six transmembrane (TM) helices and one pore domain (P-domain) in one subunit. This group contains calcium-activated and voltage gated potassium channel.

(2) 4TM/2P channels: They have four transmembrane (TM) helices and two pores (P-domain) in one subunit. They are usually designated as K_{2P} or two-pore-domain potassium channels.

(3) 2TM/1P channels: The simplest of potassium channels subunits is represented by the 2TM/1P group. They are composed of two transmembrane (TM) helices with a single pore domain (P-domain) in between and represented by inwardly rectifying potassium channel.

1.2 Inwardly rectifying potassium channels Kir2.X

More than half a century ago, the phenomenon of inwardly rectifying K^+ (Kir) currents was first described in skeletal muscle (Katz, 1949). But until 1993, Kir channel cDNAs were isolated by expression-cloning techniques. The Kir channel Kir1.1 (also denoted ROMK) and the Kir channel Kir2.1 (also denoted IRK) were cloned from the outer medulla of rat kidney and a mouse macrophage cell line, respectively (Ho *et al.*, 1993; Kubo *et al.*, 1993). The eletrophysiological properties of Kir channels show more inward current than outward current due to a reduced open probability in a depolarized membrane. Inward rectification is a strongly voltage-dependent decline of potassium conductance upon membrane depolarization producing a characteristic region of so-called ‘negative slope’ conductance (Figure 1.2), which is thought to be caused by block from intracellular polyamines and Mg^{2+}. Indeed, it is not only the negative slope conductance, but the entire inward rectification that is caused by polyamines and Mg^{2+}. Another unique attribute of Kir currents is the unusual dependence of rectification on extracellular K^+ concentration (Anumonwo & Lopatin, 2010).

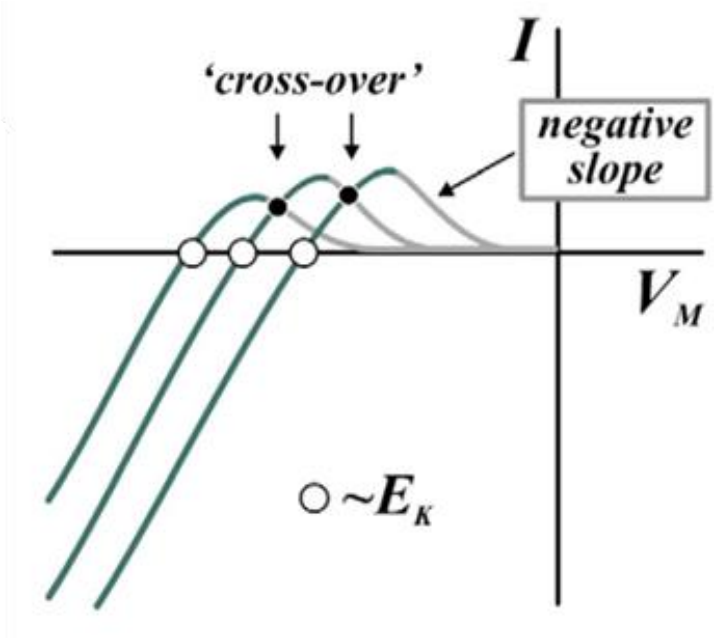

Figure 1.2 Basic characteristics of the classical inward rectification. Membrane depolarization causes a block of the Kir channel pore by intracellular polyamines and Mg^{2+} ions, leading to a voltage-dependent decline of K^+ conductance, This effect produces a region of 'negative slope' conductance. In addition, an increase in the concentration of extracellular K^+ leads to a near parallel shift of the current/voltage relationships and their 'cross-over' of the curve, because higher extracellular K^+ concentrations increase the conductance in the Kir channels (Adopted from Anumonwo and Lopatin 2010).

Kir channels conduct K^+ currents more in the inward direction than in the outward direction. Under physiological conditions, Kir channels only show outward current. They are essential in the control of resting membrane potential, coupling of the metabolic cellular state with membrane excitability, and maintenance of potassium homeostasis (Nichols & Lopatin, 1997; Abraham *et al.*, 1999).

The amplitude of the potassium current flowing through Kir channels, like all ion channels, depends on three factors: the single channel conductance (γ), the number of ion channels at the cell surface (N), the open state probability of the channels (P_0), which can be written as an formula $I = \gamma \times N \times P_0$. The observed voltage dependent changes in open probability are mainly due to block of the channels by polyamines and Mg^{2+}. So, the number of ion channels at cell surface and the open state probability of the channels are critical determinants of whole cell current carried by Kir2 channels.

1.3 The Kir2.x subfamily

Kir channel family can be classified into four subfamilies: classical Kir channels (Kir2.x), G protein-gated Kir channels (Kir3.x), ATP-sensitive K^+ channels (Kir6.x), and K^+ transport channels (Kir1.x, Kir4.x, Kir5.x, and Kir7.x) (Hibino *et al.*, 2010) (Figure 1.3). Kir channels show approximately 60% amino acid similarities between individual members within each subfamily and 40% similarities between subfamilies (De Boer *et al.*, 2010).

Inward rectifiers (Kir) share great amino acid and structural similarities in the subfamily. However, only two subfamilies, Kir2.x and Kir3.x have classical 'strong inwardly rectifying currents originally observed in cardiac and skeletal muscle (Anumonwo & Lopatin, 2010).

Heteromerization generally occurs between members in the same Kir2.x subfamily. For example, Kir2.1 can associate with any one of other Kir2.x subfamily members (Kir2.2, Kir2.3, or Kir2.4) (Preisig-Muller *et al.*, 2002) and Kir3.1 assembles with Kir3.2, Kir3.3, or Kir3.4. An exception is Kir4.1 that can form heteromers with Kir5.1 (Hibino *et al.*, 2010).

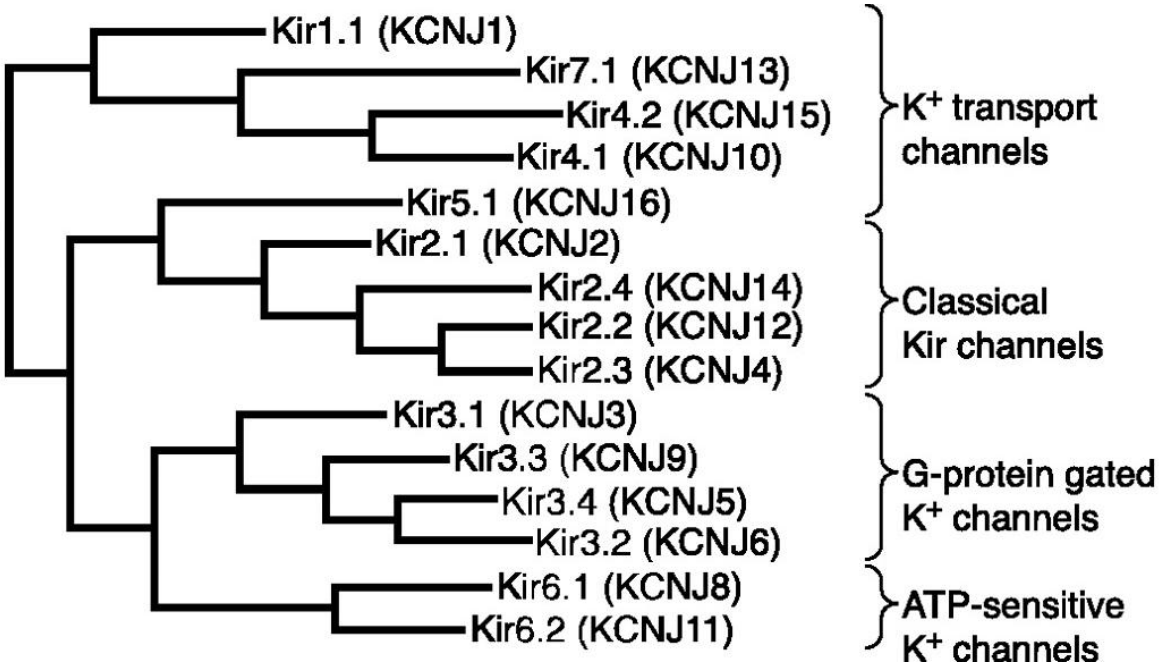

Figure 1.3 A phylogenetic tree of the human Kir channel family. Phylogenetic tree analysis of the 15 known subunits of human Kir (Adopted from Hibino et al., 2010).

1.4 Channelopathies of Kir2.1

Kir2.1 channels have been associated with a number of cardiac diseases: Andersen syndrome (long QT syndrome type 7, LQT7), catecholaminergic polymorphic ventricular tachycardia (CPVT), familial atrial fibrillation (FAF), and short QT3 (Anumonwo & Lopatin, 2010; Hibino *et al.*, 2010). Mutations on Kir2.1 channel associated with channelopathies condition (reviewed in Anumonwo and Lopatin, 2010).

More than 33 mutations in Kir2.1 are now linked with Andersen syndrome (reviewed in Anumonwo and Lopatin, 2010). Heterologous expression studies of mutant channels have shown that the mutations could lead to loss-of-function of Kir2.1 channels using. Some of the mutations lead to dominant negative effects on the K^+ current by interfering the interaction between the channels and PIP2 or by inhibiting trafficking of Kir2.1 to plasma membrane (Shieh *et al.*, 2000).

Andersen syndrome is also called Long QT syndrome type 7 (LQT7). Long QT syndromes are characterized by a prolongation of the QT interval on the electrocardiogram (ECG) in individuals with structurally normal hearts. They can cause polymorphic ventricular tachycardia, syncope and sudden death. So far, LQTS is classified as LQT1–13 according to genetically identified abnormalities.

1.5 Structure of Kir2.1 Channels

X-ray crystallography has provided more details of the 3D structure of potassium channels down to the atomic level. Doyle et al., firstly reported the crystal structure of an ion selective filter, using the bacterial K^+ channel KcsA as a model system (Doyle *et al.*, 1998). This research provided us with broader understanding mechanisms of ion selection, permeation and gating.

Recently, cytoplasmic domain structures of mouse Kir2.1 channels (Figure 1.4) (Pegan *et al.*, 2005), were analyzed in detail and revealed an intrinsically flexible cytoplasmic pore facing loop. These loops compress at the cytoplasmic pore to ~3 Å, and shape a girdle around the central pore axis. The girdle is composed of a loop between βH and βI strands, which is called the G-loop. G-loop could make the narrowest part of the ion conduction pathway in the cytosolic region. The narrowest portion of the G-loop is composed of by Ala306

and to a lesser extent by Glu299, Gly300, Met301, and Met307. In additional, di-aspartate (Asp255 and Asp259) in the C-terminus of Kir2.1 strongly influences inward rectification (Pegan *et al.*, 2005).

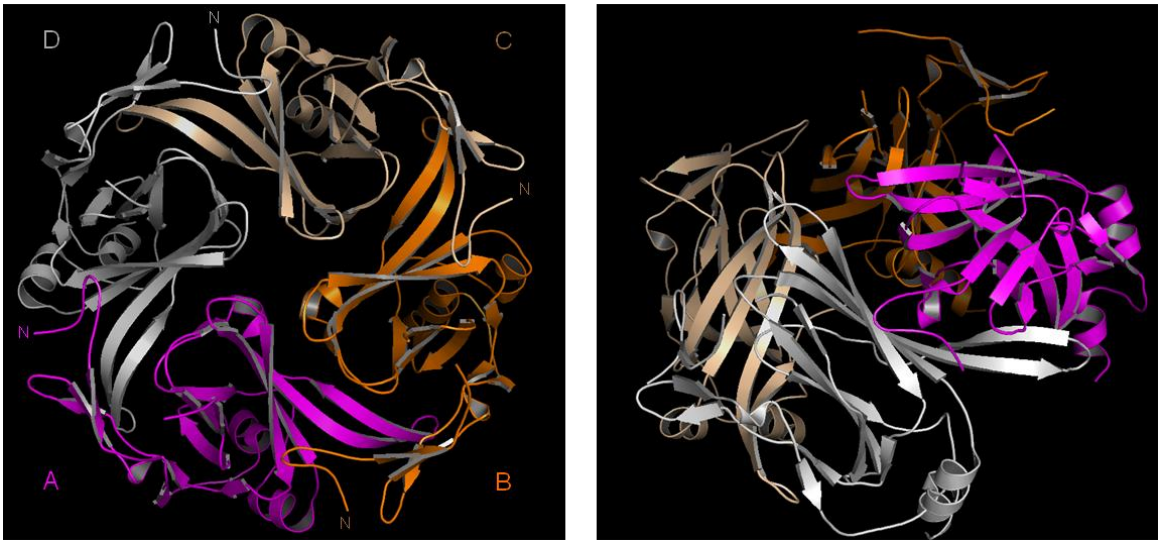

Figure 1.4 View of molecular surface of Kir2.1 channel. On the left, the cytosolic pore region viewed from the top (membrane to cytoplasm). Kir2.1 tetramer with four subunits labeled A (magenta), B (orange), C (wheat), D (grey). Note that the N-terminal region of the Kir2.1 interfaced with C-terminal segment of neighboring subunit (clockwise direction). On the right, the cytosolic pore region viewed from side, modified from Pegan et al., 2005.

1.6 Clathrin mediated endocytosis

Endocytosis is an essential process that ensures delivery of extracellular molecules or membrane-localized proteins to the cytoplasm. So far, several modes of endocytosis have been described, including clathrin-dependent endocytosis, caveolin-dependent endocytosis, clathrin and caveolin-dependent endocytosis (Doherty & McMahon, 2009; McMahon & Boucrot, 2011). In caveolin-dependent endocytosis model, caveolae are a described to form of lipid rafts, with flask shaped morphology, which is generated by assembly of caveolin coats. Apart from clathrin and caveolin dependent endocytosis, there are other models of endocytosis. For example, macropinocytosis (“cell drinking”), which usually is accompanied by membrane ruffling, the invagination of the plasma membrane to form a pocket, which then pinches off into the cell to form a vesicle filled with a large volume of extracellular fluid and its contents. Here, clathrin dependent endocytosis will be discussed in greater detail below.

Clathrin dependent endocytosis involves formation of clathrin-coated pits (CCP) and bud formation, fully formed and invagination of clathrin-coated pits, and

pinching-off of the pits to form intracellular clathrin coated vesicles (CCV) (Grant & Sato, 2006; Sorkin & von Zastrow, 2009) (Figure 1.5).

Clathrin-dependent endocytosis is mediated and regulated by multiple proteins. But the most important players are three proteins, clathrin, the AP2 adaptor complex, and the GTPase dynamin. Clathrin is composed of three clathrin heavy chains and three light chains to form a triskelion shape.

Adaptor protein 2 complexes bind to the clathrin together with more than 20 different accessory proteins to from clathrin coated pits. The AP2 protein complexes connect the endocytotic machinery to the cargo molecules, e.g. the ion channels, by binding to typical endocytic motifs.

Transmembrane cargos are recruited to the clathrin-coated pits by interactions with the clathrin-associated AP2 adaptor complex. The cargo selection into clathrin-coated vesicles is achieved by recognition of internalization motifs in the cytoplasmic regions of cargo by the AP2 adaptor complex. The most well-known internalization signals for clathrin-mediated endocytosis are: YXXΦ, [D/E] XXXL [L/I] and FXNPXY. As the clathrin-coated vesicle invaginates, dynamin forms a spiral around its neck. Finally, GTP hydrolysis triggers a conformational change in dynamin, which causes the CCVs to pinch off from plasma membrane. Then endocytic vesicles travel to the early endosome, where they fuse. The fusion process requires the small GTPase Rab5. The early endosome plays a central role, where it is responsible for distributing the different macromolecules to different cell compartments (Bonifacino & Traub, 2003). Some vesicles then recycle to the plasma membrane either directly or indirectly via recycling endosomes. The small GTPases Rab4 and Rab11 are enriched in recycling endosomes. Some vesicles are transported from early to late endosomes and eventually to lysosomes for degradation.

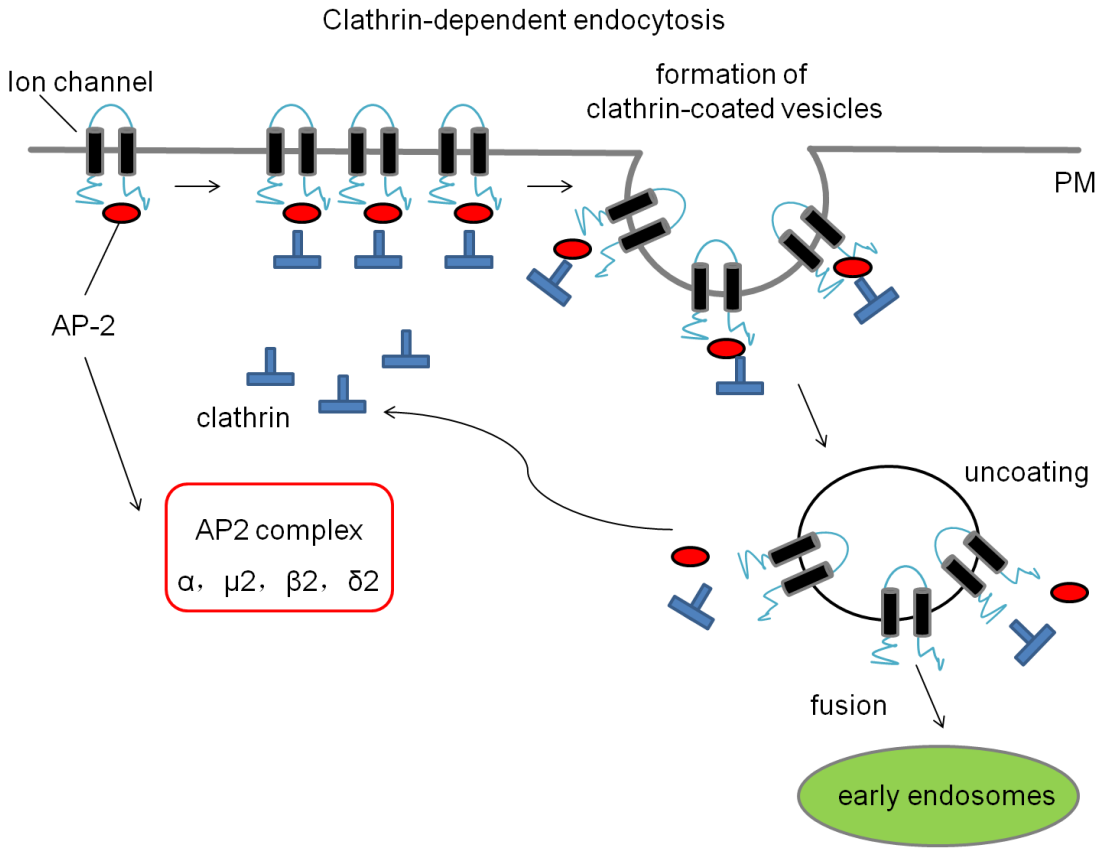

Figure 1.5. Molecular mechanism of clathrin-dependent endocytosis. Clathrin and cargo molecules (such as ion channels) are assembled into clathrin-coated pits at cell surface together with an adaptor protein complex AP-2 that served as a bridge between the receptors and clathrin, following in the formation of mature clathrin-coated vesicles (CCVs). CCVs are then actively uncoated and transported to early / later / recycling endosomes (modified from Grant and Sato, 2006).

Clathrin dependent endocytosis and caveolin-dependent endocytosis are the most widely studied in potassium channel endocytosis. Clathrin dependent pathways in different potassium channels have recently been established. For example, In Kir2.3 channels, a tandem di-hydrophobic motif (^{413}II^{414}) mediates clathrin-dependent endocytosis via direct binding to the AP-2 α and σ2 subunits (Mason *et al.*, 2008; Ortega *et al.*, 2012). In Kir1.1 (ROMK) channels, clathrin adaptor molecule autosomal recessive hypercholesterolemia (ARH) drives endocytosis via clathrin-coated vesicles and in an NPNF motif dependent manner (Zeng *et al.*, 2002; Fang *et al.*, 2009).

1.7 Overview of endocytosis of Kir2.1

The current conducted by any channel is directly proportional to the number of channels at the cell surface. The surface expression of channels can be

controlled at various anterograde trafficking steps along the biosynthetic or retrograde trafficking pathways.

As for retrograde trafficking, to date, especially endocytosis of Kir2.1 has been associated with phosphorylation of tyrosine 242, mitogen-activated protein kinases (MAPK) activation, GTPase Rho, GTPase Rac1, activity or PDZ interaction (Tong et al., 2001; Hofherr et al., 2005; Giovannardi et al., 2002; Jones, 2003; Boyer et al., 2009; Leonoudakis et al., 2004; Vaidyanathan et al., 2013).

In Xenopus oocytes, an initial study has reported that tyrosine 242 of Kir2.1 is involved in clathrin mediated endocytosis, by a tyrosine phosphorylation mechanism (Tong *et al.*, 2001). However, the function of tyrosine 242 of Kir2.1 is still a matter of debate. As Hofherr et al., showed that tyrosine 242 of Kir2.1 regulate the forward trafficking of Kir2.1 from the Golgi complex to cell surface in Opossum kidney (OK) cells (Hofherr *et al.*, 2005). The different effect could result from different model system (Xenopus oocytes vs. mammalian cell line).

Furthermore, Giovannardi et al., have shown that Mitogen-activated protein kinases (MAPK) activation stimulated removal of Kir2.1 from the membrane (Giovannardi *et al.*, 2002). Another study by Jones showed that a small GTPase, Rho, might be crucial for internalization and recycling of Kir2.1 in tsA201 cells (Jones, 2003). Interestingly, Boyer et al found that a dominant-negative mutant of the small G-protein Rac1 increased the surface expression of Kir2.1 channels, probably by interfering with endocytosis in HEK293T cells (Boyer *et al.*, 2009).

Leyland et al., have also reported that co-expression of postsynaptic density-93 (PSD-93) resulted in cell surface suppression of internalized Kir2.1 channels (Leyland & Dart, 2004). Leonoudakis et al., have shown Kir2 channels also contain PDZ binding motifs, and interact with a number of PDZ domain-containing scaffolding proteins that could affect trafficking and channel stabilization in the plasma membrane (Leonoudakis *et al.*, 2004).

Recently, Vaidyanathan et al., have reported that caveolin 3 mutations affect Kir2.1 current density by decreasing cell surface expression of Kir2.1. Caveolin 3 mutations are also associated with the LQT syndrome phenotype (Vaidyanathan *et al.*, 2013).

1.8 The goal of our study

In our study we focused on the endocytosis of Kir2.1. We pursued four aims. First, we tried to determine whether Kir2.1 undergoes constitutive internalization. Second, we investigated whether Kir2.1 is internalized by clathrin and dynamin dependent endocytosis. Third, we tried to define the potential endocytic motifs in Kir2.1. Finally, we investigated whether Kir2.1 is targeted to the endosome-lysosome pathway and to the endosomal recycling pathway.

These studies provide some more detailed insights into the mechanism of endocytosis of Kir2.1 and improve our understanding concerning how cytoplasmic signals regulate Kir2.1 trafficking.

These objectives were met in collaboration with several colleagues, whose contributions are acknowledged. CD8 reporter assays and Co-IP were done by Dr. Vijay Renigunta. These data are included in the results section of this thesis to provide a complete overview of the study. Cell surface assay, Imaging, antibody uptake assay, biotinylation internalization assay and voltage clamp were performed by me with the great help of Dr. Vijay Renigunta, Dr. Thomas Fischer, Dr. Günter Schlichthörl, Dr. Marylou Zuzarte.

2. Materials and Methods

2.1 Materials

2.1.1 Equipments

Name	Company
Agarose gel electrophoresis system	Pharmacia biotech
Centrifuge, big	Biofuge FS 28, Thermo Scientific
Centrifuge, small	Biofuge fresco, Heraeus Heraeus Fresco 17, Thermo Scientific
Fluorescence microscope	ZEISS or Olympus
Digital pH meter	WTW
Glass capillaries for injection 3.5	Replacement Tubes #3 - 00 - 203 - G/X, Drummond Scientific Company
Light microscope	MF-83, Narishige Scientific Instruments Lab.
Luminometer	Glomax, Promega
Micromanipulator	Nanoject II, Drummond Scientific Company
Micropipette Puller	DMZ Universal Puller, Zeitz
PCR Machine	MJ Mini Personal Thermal Cycler, Bio-Rad T100 Thermal Cycler, Bio-Rad
Power supply	Electrophoresis Power Supply EPS 200, Pharmacia Biotech
SDS gel system	BIO-RAD
Spectrophotometer	Nanodrop 2000c, Thermo Scientific
Western blot apparatus	BIO-RAD

2.1.2 Chemicals and Reagents

Name	Company
Acrylamide/Bisacrylamide Solution (30%; 37,5:1)	Carl Roth
Agarose	Carl Roth
Acetic acid	Merck
Albumin fraction V	Carl Roth
Ampicillin	Carl Roth
Bromophenol blue	Roth

Biotin	Pierce
Bovine serum albumin (BSA)	Roth
Collagenase	Roth
Dimethylsulfoxide (DMSO)	Sigma
dNTPs (100 mM)	Thermo-scientific
Dithiothreitol (DTT)	Sigma
Ethylenediamine tetraacetic acid (EDTA)	Sigma
Ethylene glycol tetraacetic acid (EGTA)	Sigma
Ethanol	Roth
Gentamycin	Sigma Aldrich
Glycine	Roth
Glucose	Sigma
Glutathione	Sigma Aldrich
Glycerol	Sigma Aldrich
Gelred	Biotium
Iodoacetamide	Sigma
Micropipette puller	DMZ Universal Puller, Zeitz
Nitrocelulose Membrane	GE health care
Phenol	Roth
Potassium chloride (KCl)	Roth
Protease inhibitor cock tail	Roche
RNase free water	Bioloine
Sodium chloride (NaCl)	Roth
Sodium hydroxide (NaOH) pellets	Riedel-deHaen
Sodium Dodecyl Sulfate (SDS)	Roth
N´N´N´N Tetramethylethyldiamine (TEMED)	Roth
Tris-Base	Roth
Theophylline	Sigma Aldrich
Tween 20 (Polyoxyethylenesorbitan monolaurate)	Roth
Triton X-100	Sigma Aldrich

2.1.3 Buffer and Solutions

Buffer and Solution	**Components**		
10xTAE (Tris/acetate/EDTA) electrophoresis buffer	108 g	Tris base	
	54 g	Glacial acetic Acid	
	0.5 M	EDTA (pH 8.0)	40 mL
	Filtered water to total volume 1 L		

10x PBS (Phosphate-buffered saline)	1.5 M NaCl 52 mM $Na_2HPO4\text{-}2H_2O$ 17 mM KH_2PO4 Filtered water to total volume 1L, adjust pH 7.5
Western blotting buffer recipe	5.82 g Tris 2.93 g Glycine 0.375 g or 3.75 mL 10%SDS 200 ml methanol Filtered water to total volume 1 L
Stacking gel buffer	37,86 g/L Tris-HCl (PH=6.8) Filtered water to total volume 1 L PH 6.8
Seperation gel buffer	1.125 M Tris-HCl (PH=8.8) 30% Sucrose Filtered water to total volume 1 L PH 8.8
10×SDS-PAGE electrophoresis buffer	1.5 M Tris 52 mM Glycine 17 mM SDS Filtered water to total volume 1 L， PH =7.3 (No need to adjust PH)
SDS gel-loading buffer (2X)	Tris-Cl (pH 6.8) 125 mM SDS (sodium dodecyl sulfate; electrophoresis grade) 4% (w/v) bromophenol blue 0.01% (w/v) glycerol 20% (v/v) DTT (dithiothreitol) 100 mM
Kanamycin	Storage concentration 30 mg/mL Working concentration 30 µg/mL
Ampicillin	Storage concentration 100 mg/mL Working concentration 50 µg/mL
LB medium	5 g (Mixture: Trytone,Yeast extract and NaCl) /200 mL
LB Agar	8 g (Mixture: Trytone,Yeast extract, NaCl and Agar) /200 mL
ND 96 (10x)	960 mM NaCl, 20 mM KCl, 18 mM $CaCl_2$, 10 mM $MgCl_2$, 50 mM HEPES ad 1 L H2O, adjusted to pH 7,5 with NaOH
ND 96 (1x) A B	1x ND96 supplemented with 90 mg/L theophylline, 50 mg/L Gentamycin and NaPyruvat 275 mg/L

Solutions for Surface Biotinylation assay

Name	Components
Biotin labeling solution	1.5-mg/ml Sulpho-S-S-biotin
Glycine solution	50-mM glycine
Internalization buffer	10-mM glucose
Glutathione buffer	50-mM glutathione, 75-mM NaOH, 75-mM NaCl, 1-mM EDTA, 0.1% BSA, pH 9.0
Iodoacetamide solution	5-mg/ml iodoacetamide
Extraction buffer	50-mM Tris–HCl, pH 7.4, 2-mM EDTA, 2-mM EGTA, 100-mM NaCl, 1% (w/v) Triton X-100, 1× protease inhibitor
Reducing sample buffer	25-mM sodium bicarbonate (pH 10.4), 4% SDS, 0.2% bromophenol blue, 20% glycerol plus 100-mM DTT

2.1.4 Antibodies

Antibody	Producer
Monoclonal anti-CD8 primary	Dianova
Alexa-488-conjugated anti-mouse antibody	Jackson ImmunoResearch
Alexa-594-conjugated anti-mouse antibody	Jackson ImmunoResearch
Anti-mouse IgG, horseradish peroxidase conjugate	Jackson ImmunoResearch
Rat monoclonal anti-HA antibody	Roche
Mouse monoclonal anti-HA antibody	Roche

2.1.5 Cell Lines

Cell line	Characteristic	Source
COS 7	Adherent	Simian fibroblasts
HeLa	Adherent	Cancer cell

2.1.6 Cell culture supplements

Cell culture supplements	Company
DMEM high glucose with L-Glutamin	PAA
Fetal Calf serum (FCS)	PAA
Penicillin/Streptomycin	PAA
Phosphate buffered Saline	Gibco
Trypsin/EDTA	PAA
Jetprimer	Polyplus

2.1.7 DNA Oligonucleotides

All DNA oligonucleotides were purchased either from Invitrogen or Sigma-Genosys.

Primer	Sequence
Human Kir2.1 LL231AA for	GTT CGA GCA CAG GCC GCC AAA TCC AGA ATT
Human Kir2.1 LL231AA rev	AAT TCT GGA TTT GGC GGC CTG TGC TCG AAC
Human Kir2.1 Y242A for	TCT GAA GGG GAG GCT ATC CCT CTG GAT
Human Kir2.1 Y242A rev	ATC CAG AGG GAT AGC CTC CCC TTC AGA
Human Kir2.1 Y242F for	TCT GAA GGG GAG TTT ATC CCT CTG
Human Kir2.1 Y242F rev	CAG AGG GAT AAA CTC CCC TTC AGA
Human Kir2.1 Y326A for	TGG GGC CAC CGC GCA GAG CCT GTG CTC
Human Kir2.1 Y326A rev	GAG CAC AGG CTC TGC GCG GTG GCC CCA
Human Kir2.1 YY336AA for	GAA GAG AAG CAC GCA GCA AAA GTG GAC TAT
Human Kir2.1 YY336AA rev	ATA GTC CAC TTT TGC TGC GTG CTT CTC TTC
Human Kir2.1 Y341A for	TAC AAA GTG GAC GCG TCC AGG TTC CAC
Human Kir2.1 Y341A rev	GTG GAA CCT GGA CGC GTC CAC TTT GTA
Human Kir2.1 Y341F for	TAC AAA GTG GAC TTC TCC AGG TTC CAC
Human Kir2.1 Y341F for	GTG GAA CCT GGA GAA GTC CAC TTT GTA

2.2 Methods

2.2.1 Polymerase chain reaction (PCR) reactions

All PCR reactions were carried out by a GenAmp PCR System 9600 (Applied Biosystems) or Bio-rad T100 Thermal cycler as follows.

PCR reaction (50 µl)	
10x PCR buffer	5 µl
dNTPs (2mM each)	5 µl
Primer for & rev (100 pmol/µl)	5 µl each
DMSO (optional)	2 µl
Template DNA	25-100 ng
Pfu polymerase	1 µl (2.5 U)
RNase - DNase free water to total volume	50 µl

Thermocycling condition for PCR reaction

Cycling condition	**Cycle**	**Temperature**	**Time**
Activation of Hot-start	1	95 ℃	2 min
Denaturation	25-30	95 ℃	30 sec
Annealing		55 ℃	40 sec
Extension		72 ℃	750 bp per min
Final extension	1	72 ℃	10 min
Hold		4 ℃	

2.2.2 Site directed in vitro mutagenesis

Quick-Change™ Site-Directed Mutagenesis Kit (Stratagene) was used to introduce amino acid exchanges, point mutations etc. Pfu Turbo polymerase was used to amplify the whole plasmid using two complementary primers, both of which contained the desired mutation. The primers were designed according to manufacturer's protocol. The mutagenic primers were extended during the

thermal cycling by the Pfu Turbo DNA polymerase. Their incorporation in the synthesized DNA generated a mutated plasmid.

PCR reaction (15 µl)	
10x PCR buffer	1.5 µl
25mM dNTPs	0.3 µl
Primer for& rev (10 mol/µl)	0.45 µl each
DMSO (optional)	1.5 µl
Template DNA	50-100 ng
Pfu Turbo polymerase	0.3 µl
RNase - DNase free water to total volume	15 µl

Thermocycling condition for PCR reaction

Cycling condition	**Cycle**	**Temperature**	**Time**
Activation of Hot-start	1	96 ℃	30 sec
Denaturation	18	96 ℃	30 sec
Annealing		50-55 ℃	1 min
Extension		72 ℃	18 min
Final extension	1	60 ℃	2 min
Hold		4 ℃	

Parental methylated dsDNA was digested by incubating for one hour at 37°C with 1 µl of DpnI (10 U/µl). Following this, amplification was checked on 1% agarose gels. Amplification of the mutated DNA was performed by transforming 3 µl of digested PCR products into competent *Ecoli* DH5α, which were then plated on LB agar plates with suitable antibiotic.

2.2.3 Gel Extraction / PCR purification of the DNA

The DNA samples were mixed with loading buffer and loaded onto the 1% agarose gels. The electrophoresis was performed for 30 min at 80 V. To visualize DNA, the gels were treated with GelRed (1:10,000). Under UV light, the size of DNA fragments was determined by a DNA molecular weight

standard. DNA was purified using peqGOLD Gel Extraction Kit (peqlab) according to the manufacturer's instructions. The DNA fragment was excised from the gel and dissolved in an equivalent volume of binding buffer at 60°C with shaking for 7 min. The DNA agarose solution was applied onto DNA binding column and the flow-through collected by centrifugation at 10000 × g for 1 min was discarded. The column was washed twice with 600 µl of CG buffer followed by elution with 30-50 µl elution buffer.

For purification of PCR products, an equal volume of CP buffer was added to the PCR reaction and then PCR reaction/CP buffer was bound to the column followed by subsequent washing steps (2x) with 750 µl CG buffer and elution with 30-50 µl elution buffer.

2.2.4 DNA restriction and ligation reactions

Restriction reactions were carried out at 37°C for 1-2 hours with FAST digest restriction enzymes from Fermentas. All restriction digestions were performed according to the manufacturer's instructions. Ligation reactions were performed with T4 DNA ligase (New England Biolabs) at 4°C overnight or room temperature for 1 hour.

Restriction reaction (10 µl)	
Restriction buffer 10×	1 µl
DNA	0.2-2 ug
Restriction enzyme	1µl 10 (U/µl)
RNase - DNase free water to total volume	10 µl

Ligation reaction (10 µl)	
Ligase buffer	1 µl
Digested vector 0.5-1ug	2 µl
DNA fragment of interest	6 µl
T4 DNA ligase 400 000U/µl	1 µl

2.2.5 DNA transformation into *E. coli*

The ligated DNA was transformed into DH5α sub-cloning efficiency competent cells following the manufacturer's protocol. For each transformation 50 µl of competent cells were mixed with 5-10 µl of ligated DNA and incubated on ice for 30 min. The cells were then subjected to heat shock at 37°C for 30-45 sec and kept on ice for 2 min. Following this, 1 ml of LB medium was added and the cells were incubated at 37°C for 1 hour at 250 rpm. Thereafter, the cells were centrifuged and plated on the appropriate antibiotic containing LB agar plates. The plates were inverted and placed in the 37°C bacteria incubator overnight.

2.2.6 Preparation of plasmid DNA

For small scale plasmid preparations ('mini prep') a single clone was picked and incubated for overnight culture of 2.5 ml volume with vigorous shaking at 200rpm. The plasmid DNA was isolated by Mini Kit Spin from OMEGA. The cells were centrifuged at 10000 × g and resuspended in 250 µl solution 1 containing RNase A. 250 µl of solution 2 and 350 µl of solution 3 were added and mixed subsequently. This mixture was centrifuged at 13,000 × g for 10 min and the supernatant was added to a DNA binding column. The column was washed with 500 µl of HB buffer followed by 750 µl of DNA wash buffer. The column was centrifuged for 3 min at 13,000 × g for drying and the plasmid DNA was eluted with 30 µl of elution buffer. All the buffers and the columns were provided in the kit.

Large scale plasmid preparations were carried out by 'plasmid Midi kit protocol' from Qiagen. A single colony was picked for incubating a 50 ml overnight culture with an appropriate antibiotic. The cells were centrifuged at 5300 rpm for 15min and resuspended in 4 ml buffer P1 containing RNase. To this, 4 ml of buffer P2 was added and incubated for 3 min followed by addition of 4 ml buffer S3. The mixture was passed through a filter to collect the cleard lysate followed by 2 mL Buffer BB. And then the flow through containing the plasmid DNA was bound to a DNA binding column. The column was washed with 0.7 ml buffer ETR followed by 0.7 ml buffer PE. The column was centrifuged for 1 min at

13,000 × g for drying and the plasmid DNA was eluted with 200µl Buffer EB. All the buffers and the columns were provided in the kit.

2.2.7 DNA sequencing

All sequences were validated by SEQLAB Sequence Laboratories Göttingen GmbH (Applied Biosystems). The sequence samples were prepared according to the protocol provided by the company.

2.2.8 cRNA synthesis

cRNA synthesis was performed by mMESSAGE mMACHINE kit (Ambion) according to the user's manual. The DNA of human Kir2.1 constructs was subcloned into the Xenopus oocyte expression vector pSGEM. Plasmids were linearized by digesting with the restriction enzyme Nhe-I for 2 hours at 37°C. The purified and linearized constructs were then used as templates for in vitro transcription reaction as shown below:

The reaction mixture	
2 X NTP/cap	7.5 µl
2 X reaction buffer	1.5 µl
Linearied vector 5 overhang	(0.8 µl/ µl)
Enzyme mixture	1.5 µl
RNase - DNase free water to total volume	15 µl

Following in vitro transcription, the cRNA was subjected to LiCl precipitation, which effectively removed unincorporated nucleotides and most proteins. The RNA was washed with 70% EtOH and resuspended in 20 µl RNase - DNase free water. Finally optical density (OD) was measured at 260 nm and 1 µl of cRNA was loaded on to agarose gel to check for the quality.

2.2.9 Protein Biochemistry

2.2.9.1 Measuring protein concentration using BCA protein Assay

The BCA Protein Assay combines the well-known reduction of Cu^{2+} to Cu^{1+} by protein in an alkaline medium with the highly sensitive and selective colorimetric

detection of the cuprous cation (Cu^{1+}) by bicinchoninic acid. In the BCA protein assay, two-fold serial dilutions were used for BSA standard protein (linear range of 0.0625 to 2 mg/ml). Fresh working reagent (50A:1B) was prepared for all the standards and samples. 10 µl of standards were mixed with 200 µl of working reagent in a tube together with a blank control (dilution buffer with working reagent). Then both the standards and sample tubes were incubated at 60°C for 5 min and subsequently cooled to room temperature for making a standard curve. Quantification of samples were performed by using NanoDrop 2000c (Thermo).

2.2.9.2 Co-Immunoprecipitation

For immunoprecipitations, HA-tagged (YPYDVPDYALE, between residues 236 and 237 amino acids) µ2 subunit of AP2 complex cloned in to pcDNA3.1 (Invitrogen, Carlsbad, CA, USA) mammalian expression vector was co-transfected with EGFP-tagged Kir2.1 constructs in HeLa cells. 48h after transfection cells were washed with PBS, collected using centrifugation and extracted with lysis buffer containing 50 mM Tris–HCl, pH 7.4, 150 mM NaCl, 1 mM EDTA, 1% NP-40, 0.25% Na-deoxycholate, and 10 µL/mL protease-inhibitor cocktail (Sigma, Germany). GFP-tagged Kir2.1 constructs were immunoprecipitated overnight at 4°C with mouse monoclonal anti-GFP, clone 9E10 (Sigma), followed by incubation with protein A-sepharose beads overnight at 4°C. Immunoprecipitates were then washed extensively with lysis buffer to remove unspecific binding partners and eluted with 2 × sodium dodecyl sulphate (SDS) sample buffer, and separated on (10%-12%) SDS–polyacrylamide gel electrophoresis (PAGE) gels. Eluted proteins were visualized using rat anti-HA antibodies (clone 3F10; Roche 1:1000) or mouse anti-GFP antibody (Santacruz; 1:1000) and appropriate fluorescence-conjugated secondary antibodies (LICOR Biosciences; 1:10,000). The bands were detected using Odyssey Imaging Systems (LI-COR Biosciences).

2.2.10 Cell culture and Transfection

COS-7 or HeLa cells were grown in DMEM supplemented with 10% fetal bovine serum (Invitrogen) and 1% Pen/Strep (PAA) in 35 mm tissue culture dishes. After 24 hours, transfection was performed with 1: 2 DNA to jetPRIME reagent ratio (Polyplus). The DNA was added into jetPRIME buffer, mixed together and

then added appropriate amount of jetPRIME incubating for 10 min for complex formation. Transfection mixture was then gently dropped on the cells. After 4-6 hours, the solution was replaced by complete medium and the plates were incubated for 24-48 h.

2.2.11 Fluorescence microscopy

COS-7 cells or HeLa cells were seeded on glass-bottom Petri dishes (Wellco, Amster-dam) and transfected with EGFP-tagged Kir2.1 constructs using jetPRIME reagent (Polyplus). 24–48 h after transfection, live-cell images were acquired using an Olympus IX71 microscope equipped with a 60 (NA 1.3) or 100 (NA 1.4) Olympus PLANAPO objective, standard EGFP/Texas Red filter sets and a cooled 12-bit charge-coupled device camera (SensiCam QE; PCO, Kehlheim, Germany). During imaging, the cells were maintained at 37°C by means of an objective heater. Images were analyzed with Image Pro-Plus 4.5 (MediaCybernetics, Silver Spring, MD, USA).

2.2.12 Electrophysiology-Two-microelectrode Voltage Clamp (TEVC)

Ovarian lobes were dissected from mature Xenopus laevis anesthetized with tricaine and shaked with collagenase (1 mg/ml, Worthington, type II) in OR2 solution (82.5 mM NaCl, 2 mM KCl, 1 mM $MgCl_2$, 5 mM HEPES, pH 7.4) for 120 min. Isolated oocytes were stored at 18°C in ND96 recording solution (96 mM NaCl, 2 mM KCl, 1.8 mM $CaCl_2$, 1 mM $MgCl_2$, 5 mM HEPES, pH 7.4) plus Na-pyruvate (275 mg/L), theophylline (90 mg/L) and gentamicin (50 mg/L). Stage IV and V oocytes were injected with Kir2.1 and mutants cRNA (1 ng/per oocyte). Standard two microelectrode voltage-clamp experiments were performed at room temperature 2 days after injection of oocytes with cRNA. Microelectrodes were pulled from glass tubes backfilled with 3 M KCl and had a resistance of 0.2–1.0 MΩ. Currents were recorded by voltage ramps ranging from −120 mV to +40 mV. The holding potential was −80 mV. Data shown are based on the average current, measured at -100mV.

2.2.13 Quantitative chemiluminescence in COS-7 cells

For COS-7 cells, chemiluminescence measurement of HA tagged surface proteins has been previously described elsewhere (Margeta-Mitrovic, 2002). To quantify the cell surface expression of HA tagged Kir2.1 constructs, COS-7 cells

plated in 35 mm dishes were transfected and surface expression of all the constructs was carried out 24 hours after transfection. Cells were fixed with 4% formaldehyde in PBS (20 min), blocked in PBS with 1% fetal bovine serum (30 min), and then labeled with rat monoclonal anti HA antibody (0.2 mg/ml) antibody for 1 h, Cells were washed with blocking buffer (10 min, 5 times) and with an peroxidse-conjugated affinity-purified ($F(ab)^2$) goat anti-rat IgG antibody (0.8 µg/mL) for 20 min. After unbound antibody was removed by extensive washing (blocking buffer 10 min, 5 times and PBS buffer 10 min, 6 times). Chemiluminescence was quantitated in a TD-20/20 luminometer (Lumat LB9507, Berthold Technologies, Bad Wildbad, Germany), after 15 sec of incubation in SuperSignal ELISA Femto Maximum Sensitivity Substrate (Pierce). All steps were performed at room temperature.

2.2.14 Quantitative chemiluminescence in Xenopus Oocytes

For Xenopus oocytes, surface expression of HA-tagged Kir2.1 constructs in Xenopus oocytes was analysed as described previously elsewhere (Margeta-Mitrovic, 2002). Two days after injection of complementary RNA (cRNA) oocytes were incubated for 30 minutes in ND96 solution containing 1% BSA at 4°C to block non-specific binding of antibodies. Subsequently, oocytes were incubated for 60 min at 4°C with 1 mg/mL rat monoclonal anti-HA antibody (clone 3F10, Roche) in 1% BSA/ND96, washed six times at 4°C with 1% BSA/ND96 and incubated with 2 mg/mL peroxidase-conjugated affinity-purified $F(ab)^2$ fragment goat anti-rat immunoglobulin G antibody (Jackson ImmunoResearch) in 1% BSA/ND96 for 60 minutes. Oocytes were washed thoroughly, initially in 1% BSA/ND96 (at 4°C for 60 min) and then in ND96 without BSA (at 4°C for 15 min). Individual oocytes were placed in 20 µL SuperSignal Elisa Femto solution (Pierce) and after an equilibration period of 10 seconds, chemiluminescence was quantitated in a TD-20/20 luminometer (Lumat LB9507, Berthold Technologies, Bad Wildbad, Germany). With each construct surface expression of 8–15 oocytes was analyzed in one experiment, and at least three experiments were carried out. The luminescence produced by noninjected oocytes was used as a reference signal (negative control).

2.2.15 CD8 reporter assay

Surface expression was quantified as described previously (Margeta-Mitrovic M et al., 2000). In brief, COS-7 cells were transfected with the indicated constructs using jetPRIME. After 24 hours, cells were fixed with 4% formaldehyde in PBS for 20 min, blocked in PBS with 1% fetal bovine serum for 30 min, following wash 5 x 10min with 1x blocking solution, and then labeled with a monoclonal anti-CD8 primary (clone UCHT-4; Dianova) and a horseradish-peroxidase (HRP)-conjugated secondary antibody (Jackson ImmunoResearch). Finally, the cells were extensive washed 4 x 10min with 1x blocking solution and 5 x 10min with 1x PBS. Surface expression was measured by luminometry using a luminogenic substrate of HRP (SuperSignal; Pierce Biotechnology) as mentioned above in Method 2.2.13.

2.2.16 Antibody uptake assay

Antibody uptake assay with COS-7 cell were performed 24 h after transfection with HA-tagged Kir2.1 constructs. Cells were blocked with 1x PBS containing 5% FCS (Life technologies) for 30 min at room temperature. Channels at the cell surface were labeled with mouse anti-HA antibody (Sigma-Aldrich; 1:1000) at 4°C for 60 min. The cells were then washed extensively (3x) with 1x PBS at 4°C to remove unbound antibody. Subsequently, the labeled channels at the cell surface were allowed to internalize for variable times at 37°C. The cells were then fixed for 10 min at 4°C in PBS containing 4% paraformaldehyde. The channels remaining at the surface were labeled with a saturating concentration of Alexa Fluor 488–conjugated goat anti-mouse secondary antibody. Following cell permeabilization with 0.1% Triton X-100 for 5 min at room temperature, internalized channels were detected with Alexa Fluor 594–conjugated goat anti-mouse secondary antibody, After extensive washing with PBS buffer the coverslips were mounted on glass slides. The labeled cells were visualized using an Olympus IX71 microscope equipped with a 60× objective (PlanApo 60×/1.40 Oil, Olympus), a cooled 12-bit CCD camera (SensiCam QE, PCO, Kehlheim, Germany) and the corresponding filters for the fluorescent dyes. Images were acquired with Image-Pro Plus 4.5 (Media Cybernetics, Silver Spring, MD, USA) and analysed with NIS Elements AR 4 software (Nikon). Channel endocytic rate was quantified by using the ratio between the

fluorescence of the Alexa Fluor 488-coupled secondary antibody (green, channels at the cell surface) and the fluorescence of the Alexa Fluor 594-coupled secondary antibody (red, internalized channels).

2.2.17 Biotinylation internalization assay

Biotinylation assay for internalization was performed as described previously (Mankouri *et al.*, 2006). HeLa cells transiently transfected with HA-tagged Kir2.1 constructs were grown to 80-90% confluency in 35 mm dishes. After 4 X washes with 1× PBS (10 mM Na_2HPO_4, 2 mM KH_2PO_4, 137 mM, NaCl, 2.7 mM KCl, 1 mM $MgCl_2$ and 2.5 mM $CaCl_2$, PH 7.4) cells were biotinylated using the membrane impermeant Sulfo-NHS-SS-Biotin (1.5 mg/ml, Pierce) in PBS for 20 min on ice. Unreacted biotin reagent was quenched by washing the cells twice (5 min each) with 50 mM glycine in PBS on ice. Cells were incubated at 37°C in PBS containing with 10 mM glucose to allow internalization for 30 min.

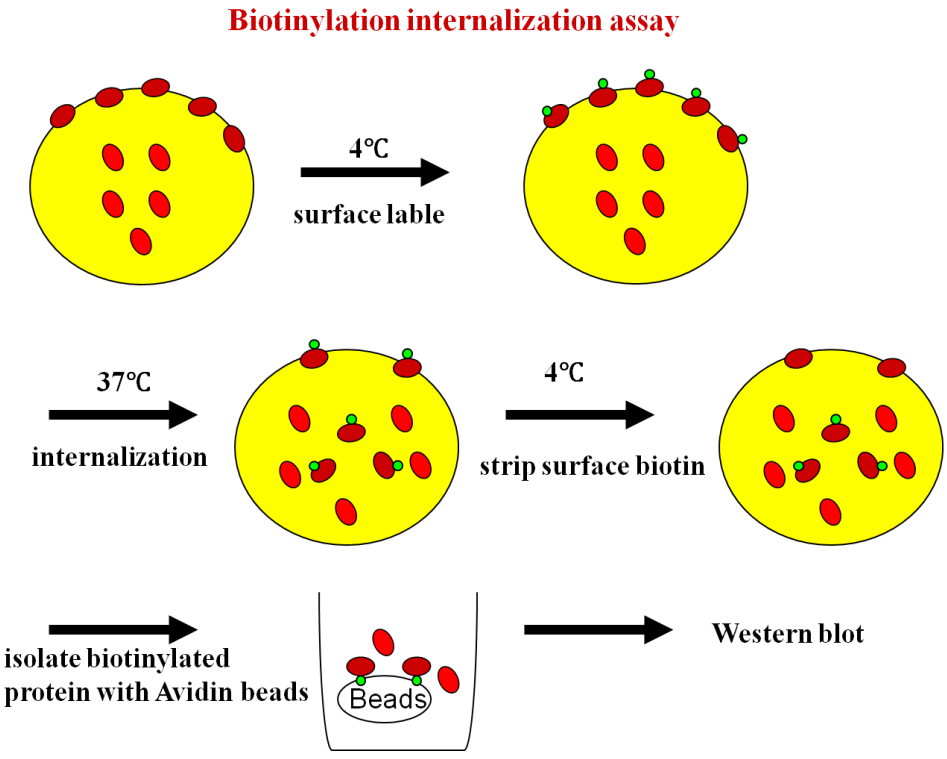

Figure 2.1 Cartoon of biotinylation internalization assay. Cells were biotinylated at 4°C or on ice to label the surface proteins and then incubated at 37°C to allow internalization of surface proteins. Following internalization, cells were quickly chilled to block internalization and the remaining surface biotin is stripped by incubation with a reducing agent. Biotinylated proteins in the lysate were absorbed on Neutravidin coated beads and the proteins in the elution buffer were detected by Western blotting (Modified from Luke Gabriel et al., 2009).

Following internalization, cells were blocked by chilling on ice immediately. The residual cell surface biotin was removed by incubating the cells with GSH buffer

containing the non-permeant reducing agent glutathione (GSH 50 mM, NaOH 75 mM, NaCl 75 mM, EDTA 1 mM, BSA 0.1%, pH 9.0) two times for 20 min each at 4°C. GSH was quenched with iodoacetamide (5 mg/ml) in PBS. Cells were then lysed in extraction buffer (50 mM Tris pH 7.4, 2 mM EDTA, 2 mM EGTA, 100 mM NaCl, 1% Triton X100, 1x protease inhibitor cocktail). After centrifugation (13,000 x g for 15 min at 4°C) supernatants containing equal amounts of protein were incubated with BSA-blocked Ultralink-neutravidin beads (Pierce) to immunoprecipitate the remaining biotinylated proteins. Following extensive washes in extraction buffer, proteins were isolated from the streptavidin beads by using reducing sample buffer (25 mM sodium bicarbonate pH 10.4, 4% SDS, 0.2% bromophenol blue, 20% glycerol, plus 100 mM DTT) at room temperature for 15 min. and then checked by SDS-PAGE and immunoblotted using rat anti-HA antibodies (clone 3F10; Roche 1:1000) and fluorescence-conjugated goat anti-rat secondary antibodies (LICOR; 1:10,000). The bands were detected using Odyssey Imaging Systems (LI-COR Biosciences).

2.2.18 Bioinformatics tools

Name	**Website**
NCBI Nucleotide BLAST	http://blast.ncbi.nlm.nih.gov
Expasy Translate Tool	http://web.expasy.org/translate
Web Map Preference	http://pga.mgh.harvard.edu/web_apps/web_map/start
ClustalW2 Mulitple Sequence Alignment	http://www.ebi.ac.uk/Tools/msa/clustalw2
NebCutter V2.0	http://tools.neb.com/NEBcutter2
ELM (Functional site prediction)	http://elm.eu.org/

3 Results

3.1 Kir2.1 undergoes constitutive endocytosis

A recombinant Kir2.1 channel containing an extracelluar hemagglutinin (HA)-tag between D114 and A115 amino acids was used. Insertion of HA tags did not alter Kir2.1 electrophysiological behavior (Figure 3.1). Therefore, the HA-tagged version of the Kir2.1 ($Kir2.1^{HA}$) construct was used in the place of wild-type Kir2.1 for all subsequent studies in order to perform both trafficking and electrophysiological studies with the same construct.

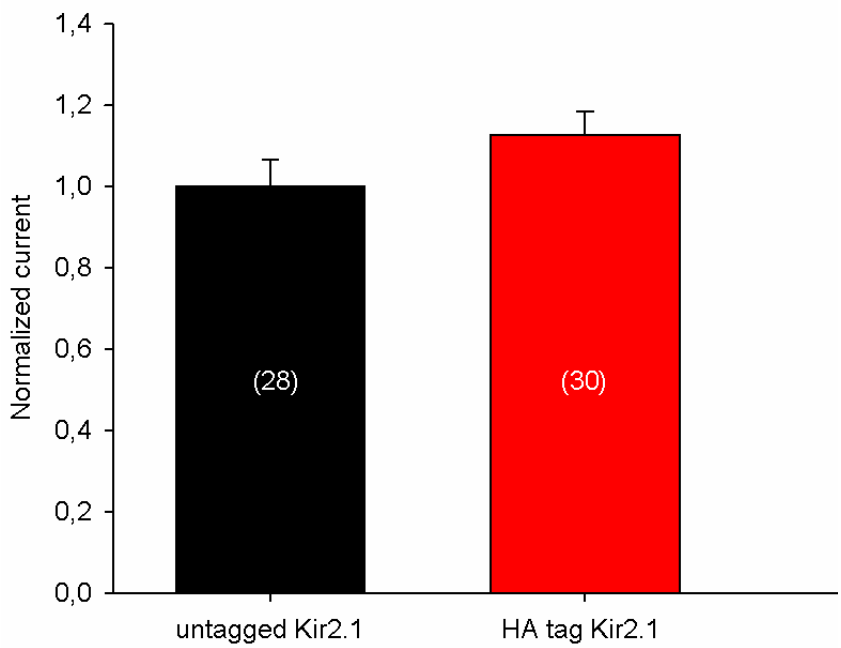

Figure3.1 Untagged and HA tagged Kir2.1 channels were expressed in Xenopus oocytes, and current was measured using two electrode voltage clamp. The number of oocytes for each condition is indicated in brackets.

To investigate whether Kir2.1 channels could undergo constitutive endocytosis, we carried out an antibody uptake assay to visualize and quantify the internalized Kir2.1 channels (Figure 3.2A).

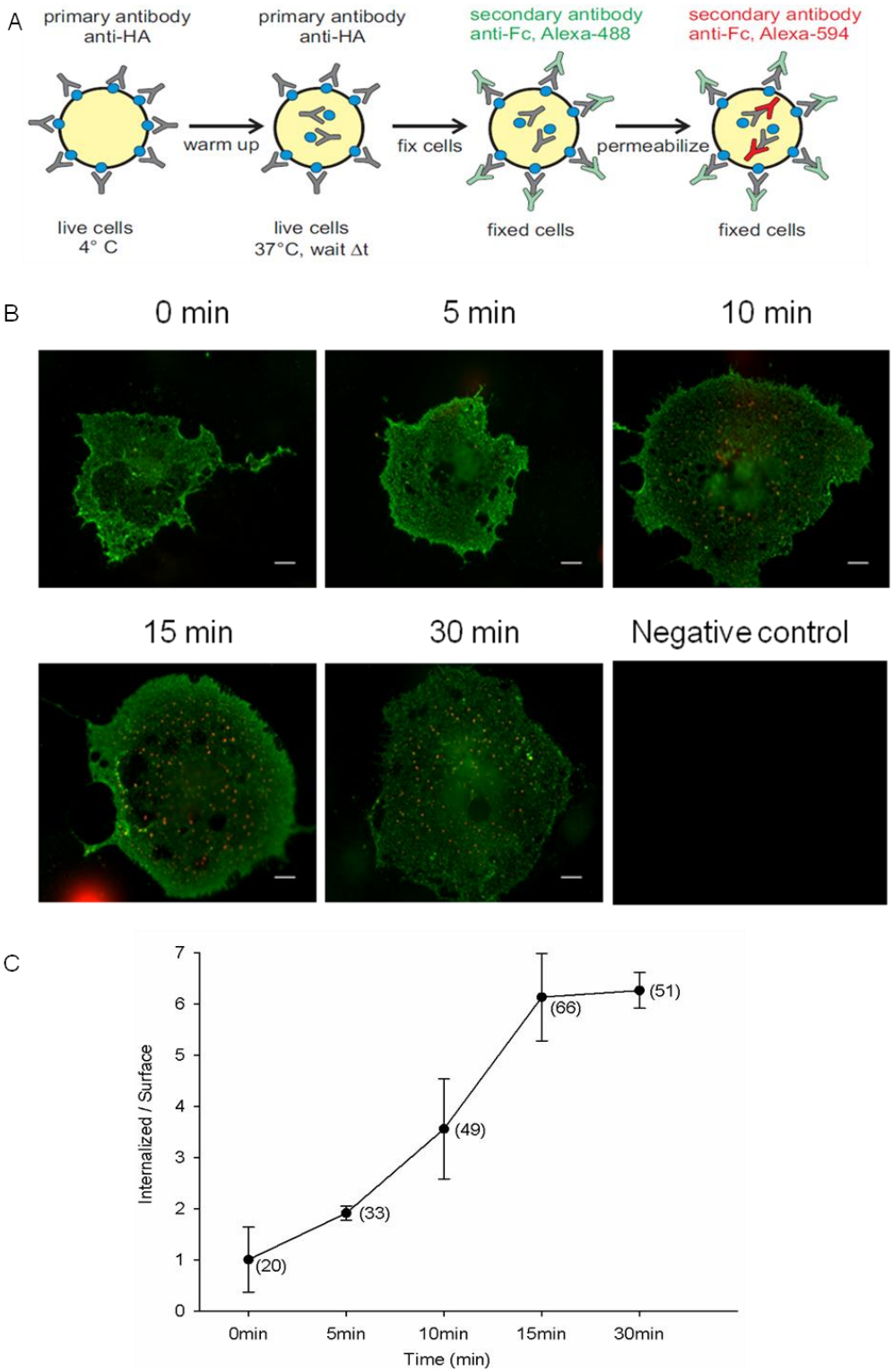

Figure 3.2 Kir2.1 undergoes constitutive endocytosis. (A) Cartoon of the antibody uptake assay. For details see Materials and methods. (B) Internalization of Kir2.1 expressed in COS-7 cells. $Kir2.1^{HA}$-expressed on the surface of COS-7 cells was labeled with a mouse anti-HA antibody and then allowed to internalize for 5, 10, 15 and 30 min. Surface Kir2.1 channels were labeled with a saturating concentration of AlexaFluor-488-conjugated secondary antibody. Internalized channels were detected with AlexaFluor-594-conjugated secondary antibody after cell permeabilization. Scale bar 10 µm. (C) The fluorescence intensity for both internalized channels and cell surface channels were quantified and shown in the time course plots (mean ± SEM). The number of cells for each condition is indicated in brackets.

To measure constitutive endocytosis of Kir2.1 channels, COS-7 cells expressing $Kir2.1^{HA}$ were incubated with an anti-HA antibody on ice (non-permissive temperature) for 1 h to achieve maximal labeling and endocytosis was triggered by raising the temperature to 37°C for desired time periods (permissive temperature). To distinguish between surface and internalized Kir2.1 channel protein, the anti-HA labeled channels that remained on the surface were detected with saturating amounts of an Alexa 488–conjugated secondary antibody (green). Internalized channels, which were labeled at the cell surface with the anti-HA antibody, were detected with a different secondary antibody, Alexa 594 (red), following cell permeabilization. As shown in Figure 3.2B, the intracellular red signal increased with time, indicating that $Kir2.1^{HA}$ underwent constitutive endocytosis. As negative controls, nonpermeabilized cells or permeabilized cells without prelabeling by the anti-HA antibody were stained by using Alexa-594, demonstrating the specificity of Alexa-594 labeling for internalized $Kir2.1^{HA}$ channels (Figure 3.2B). Quantifying the ratio of fluorescence intensity between internalized and cell surface channels (Fig. 3.2C) showed that the number of endocytosed $Kir2.1^{HA}$ channels increased with time. About 20% of the antibody-labeled surface channels were internalized within 5 min of temperature shift. An apparent maximum was reached after 15 min. These data provide direct evidence that HA tagged Kir2.1 channels undergo constitutive endocytosis in COS-7 cell.

3.2 Kir2.1 is internalized by clathrin and dynamin mediated endocytosis

We next investigated whether Kir2.1 internalization was mediated by the classical clathrin and dynamin dependent pathway using a chemiluminescence assay. We used dominant negative dynamin II (K44A), or AP180C (C-terminus of AP180, a powerful and specific inhibitor of clathrin-mediated endocytosis). Co-expression of Kir2.1 with a dominant-negative mutant of dynamin (K44A), but not wild-type dynamin, enhanced the surface expression of Kir2.1 channels by 40%. Co-expression of Kir2.1 with a truncated mutant of AP180C enhanced the surface expression of Kir2.1 by 49% (Figure 3.3A). Co-expressed EGFP and mCherry vectors were used as a negative control.

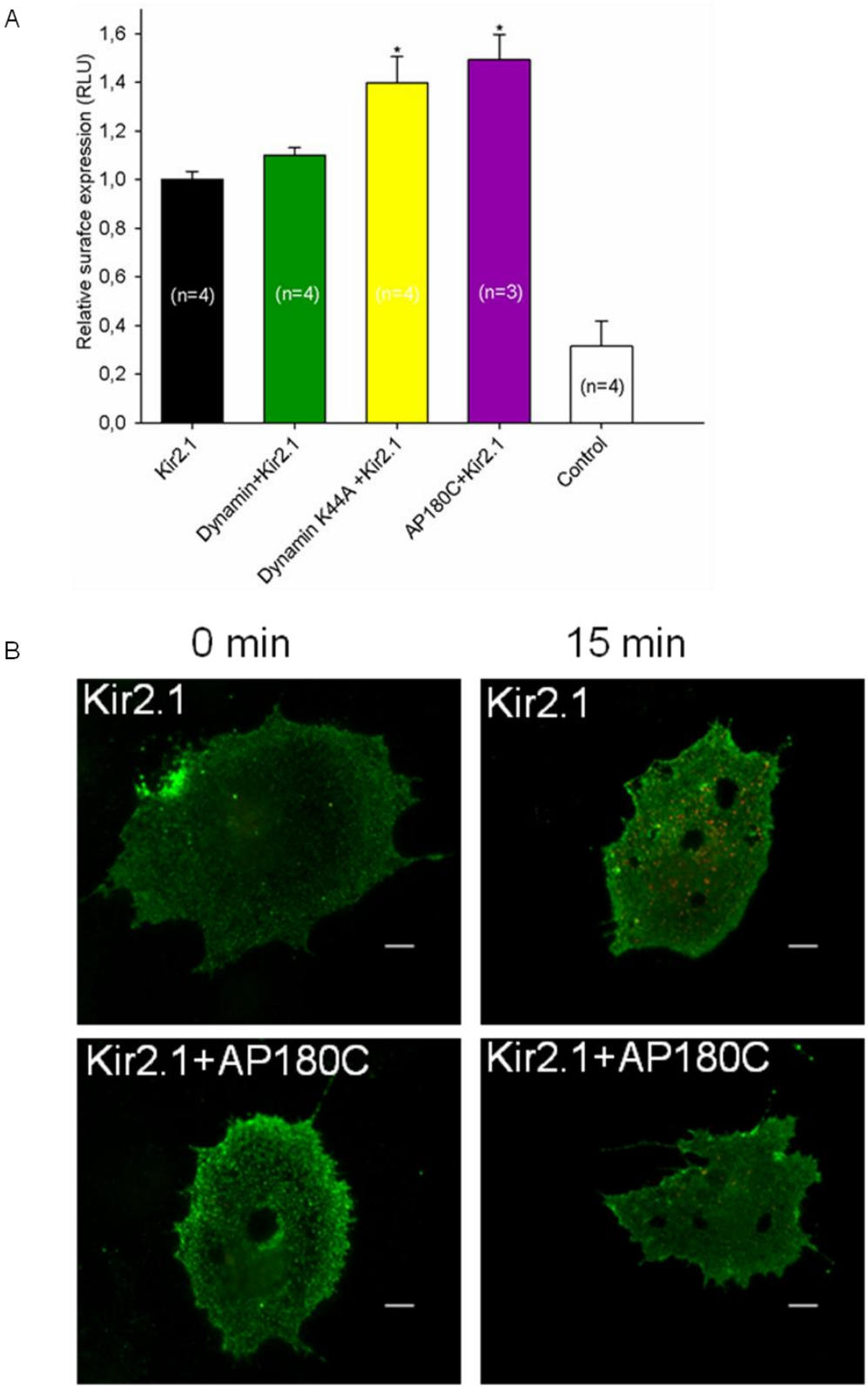

Figure 3.3 Inhibition of clathrin mediated internalization of Kir2.1. (A) Surface expression of Kir2.1 was dertermined by chemiluminescence in COS-7 cell as described in Methods. Expression of dynamin K44A or AP180C effectively inhibited the internalization of Kir2.1. Dynamin did not influence the surface expression of Kir2.1. (B) AP180C blocked the endocytosis of Kir2.1 in an antibody uptake assay. The assay was performed on COS-7 cells transfected with Kir2.1 with or without AP180C. The surface $Kir2.1^{HA}$ was labeled by AlexaFluor-488 (green), whereas the internalized HA antibody was recognized by AlexaFluor-594 (red). Scale bar, 10 μm.

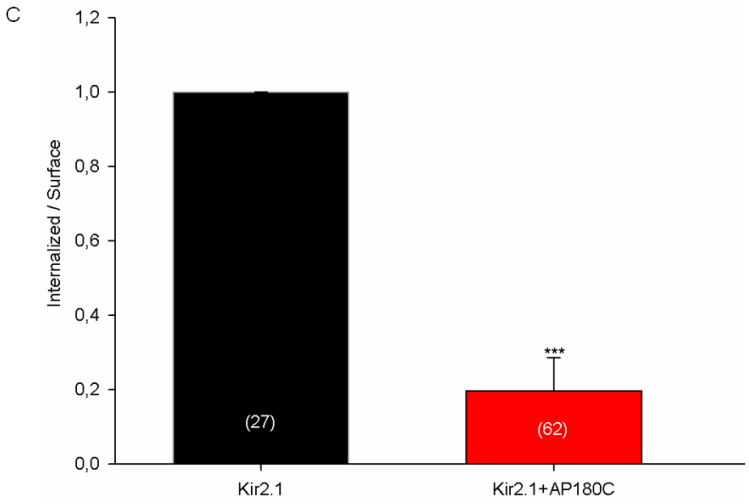

Figure 3.3 Inhibition of clathrin mediated internalization of Kir2.1. (C) Data are expressed as the ratio of fluorescence intensity of internalized channels to fluorescence intensity of cell surface channels at the 15 minute chase time. The number of cells for each condition is indicated in brackets. Significant differences from control wild type Kir2.1 were found (***P< 0.001) using the Student's t-test.

In order to make sure that increased cell surface expression was due to the inhibition of internalization, we performed co-expression experiments by using AP180C construct in an antibody update assay as described above. As seen in Figure 3.3B and 3.3C, AP180C effectively inhibited internalization of Kir2.1 by 80% compared to the COS-7 cells transfected with Kir2.1 together with a control vector (pCDNA3.1).

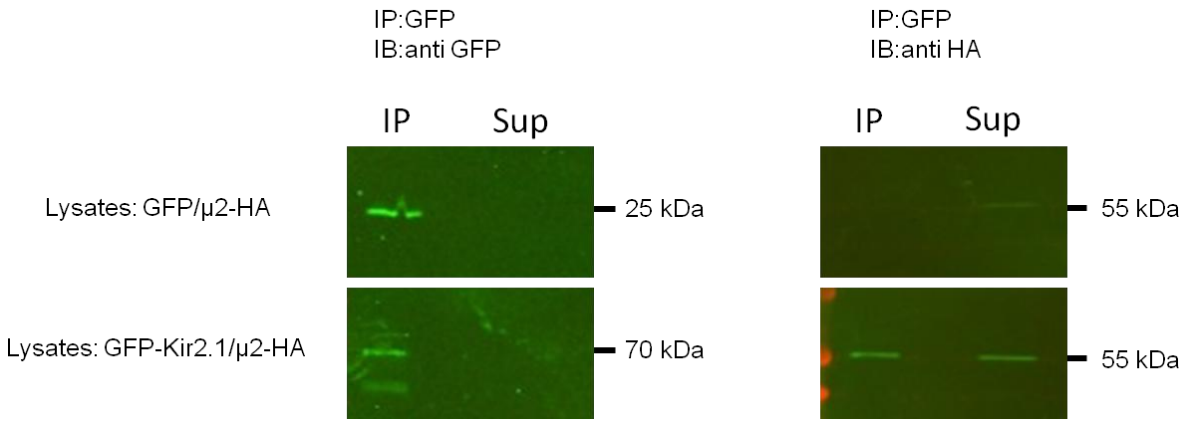

Figure 3.4 Co-immunoprecipitation of Kir2.1 and μ2 proteins heterlogously expressed in HeLa cells. The complex containing $_{EGFP}$Kir2.1 and μ2-HA was precipitated from the cell lysates with GFP antibody and a Western blot of the precipitate was probed with GFP and HA antibody. The data in Figure 3.4 are typical result of 3 independent experiments.

The interaction between Kir2.1 and μ2 subunit of the AP2 complex was confirmed by co-immunoprecipitation experiments. GFP-tagged Kir2.1 ($_{GFP}$Kir2.1) or GFP vector alone was co-expressed with HA tagged μ2 (μ2-HA)

in HeLa cells. Channel complexes were precipitated with anti-GFP antibodies and the precipitate was probed with either anti-HA (μ2) or anti-GFP (Kir2.1) antibodies. We detected both μ2 and Kir2.1 proteins in the anti-GFP immunoprecipitates of HeLa cells expressing both HA tagged μ2 and GFP tagged Kir2.1 proteins as illustrated in Figure 3.4; Whereas, no μ2 protein was detected in the anti GFP immunoprecipitates of HeLa cells expressing GFP (negative control) and HA tagged μ2. These findings clearly demonstrate that Kir2.1 might interact with the μ2 subunit of the AP2 complex. Therefore, taken together, these results further demonstrate that the internalization of Kir2.1 channel is mediated via a dynamin- and clathrin-dependent endocytic pathway.

3.3 Two novel endocytotic signals in the C-terminal region of Kir2.1 channel

We attached EGFP (enhanced green fluorescent protein) to the N-terminus of a Kir2.1 construct that also contained an extracellular HA tag (HA peptide sequence YPYDVPDYA derived from the human Influenza haemagglutinin protein) in the first extracellular loop of the channel. In this way we generated a new construct named $_{EGFP}$Kir2.1^{HA} (Figure 3.6A). $_{EGFP}$Kir2.1^{HA} currents behaved electrophysiologically as the control Kir2.1 construct without any modifications (Figure 3.5).

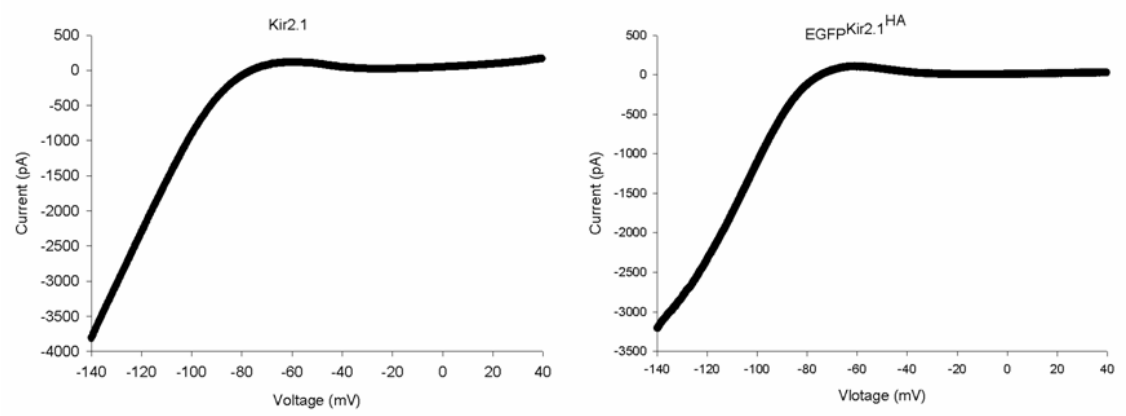

Figure 3.5 Representative current–voltage relationships from CHO cell transfected with Kir2.1 or $_{EGFP}$Kir2.1^{HA}

Five potential endocytic motifs ^{228}RAQLL^{232}, ^{242}YIPL^{245}, ^{326}YEPV^{329}, ^{336}YYKV^{339} and ^{341}YSRF^{344} within Kir2.1 intracellular C terminal tail were predicted by the website (http://elm.eu.org/) (Figure 3.6A). The ^{228}RAQLL^{232} motif represents a classical motif [D/E] XXXL [L/I] (X represent any amino acid), while the rest of

four motifs belongs to the canonical motif YXXΦ (X represent any amino acid, Φ represent is a bulky hydrophobic amino acid).

As shown in Figure 3.6B, the mutations LL231-232AA and Y326A largely reduced cell surface expression to 32% and 37% respectively compared to wild-type Kir2.1 channels. The mutation YY336AA did not significantly change the cell surface expression compared to wild type Kir2.1 channels. In contrast, the mutants Y242A, Y242F, Y341A and Y341F showed a significantly larger surface expression. Particularly, the mutants Y242A and Y341A dramatically increased cell surface expression by 31% and 58% respectively. The conservative mutant (replacement of one amino acid with a biochemically similar one, resulting in minor structural changes) Y242F and Y341F also increased by 24% and 40% respectively. To our surprise, double mutants Y242A/Y341A and Y242F/Y341F did not have additive effect at cell surface expression. Here, $_{EGFP}$Kir2.1 (without a HA tag) was used as negative control. Western blots confirmed approximately equal expression of all $_{EGFP}$Kir2.1^{HA} fusion proteins in COS-7 cells (Figure 3.6B, inset).

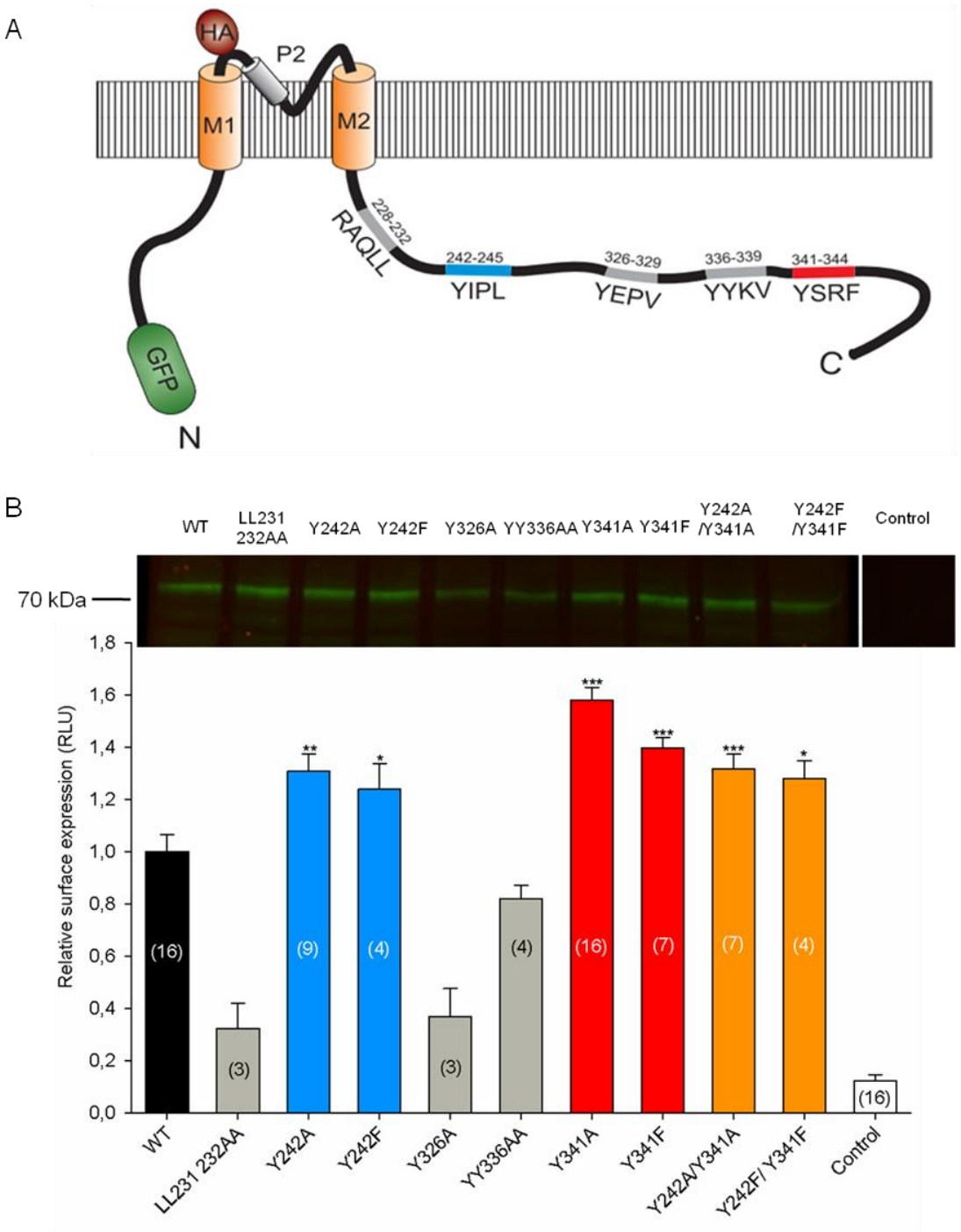

Figure 3.6 Identification of internalization signals in the C-terminal region of Kir2.1 channel in mammalian cell line (COS-7 cell or HeLa cell). (A) Graphical representation of the Kir2.1 channel subunit and its modifications used in this study. Kir2.1 has five putative endocytosis signals ^{228}RAQLL^{232}, ^{242}YIPL^{245}, ^{326}YEPV^{329}, ^{336}YYKV^{339} and ^{341}YSRF^{344} in its C-terminus. The position of two amino acids (^{242}YIPL^{245} and ^{341}YSRF^{344}) is indicated in red and green. (B) Mapping the sequence of the internalization signals. Point mutations of five putative endocytic motifs ^{228}RAQLL^{232}, ^{242}YIPL^{245}, ^{326}YEPV^{329}, ^{336}YYKV^{339} and ^{341}YSRF^{344} were made in the C-terminal domain of Kir2.1 channel. These mutants were expressed in COS-7 cells and surface expression was quantified using a chemiluminescence assay (see Materials and methods). The number of independent transfections is indicated in brackets. The value for the wild type channel was normalized to 1.0 and the mutants' data expressed relative to wild type. Data represent mean ± SEM, significant difference from wild type (*P $<$0.05, **P $<$0.01, ***P $<$ 0.001). (Inset) Western blot analysis of protein steady state levels on wild type and mutants in COS-7 cell. Another independent experiment gave similar results.

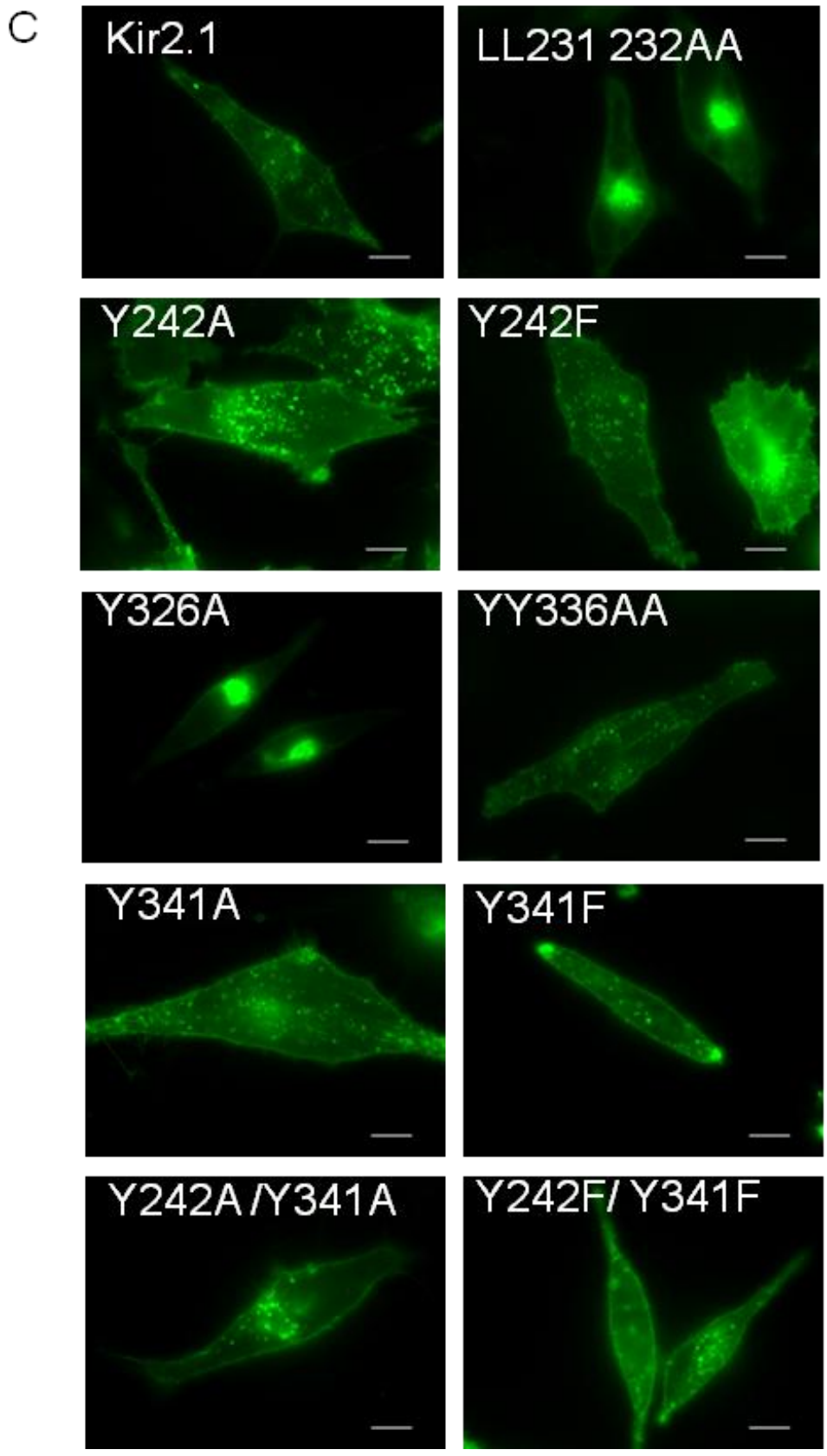

Figure 3.6 Identification of internalization signals in the C-terminal region of Kir2.1 channel in mammalian cell line (COS-7 cell or HeLa cell). (C) Representative live cell images of HeLa cells expressing EGFP-tagged Kir2.1 constructs.

To analyze the subcellular localization of the different endocytic mutants, live-cell imaging experiments were carried out in HeLa cells transfected with $_{EGFP}Kir2.1^{HA}$ constructs. The mutation of tyrosine 242 or tyrosine 341 in Kir2.1 to either alanine or phenylalanine caused an increased amount of fluorescence at the cell surface (Figure 3.6C). The double mutants Y242A/Y341A or Y242F/Y341F also revealed a more pronounced expression at the surface membrane as compared to wild-type Kir2.1 channels.

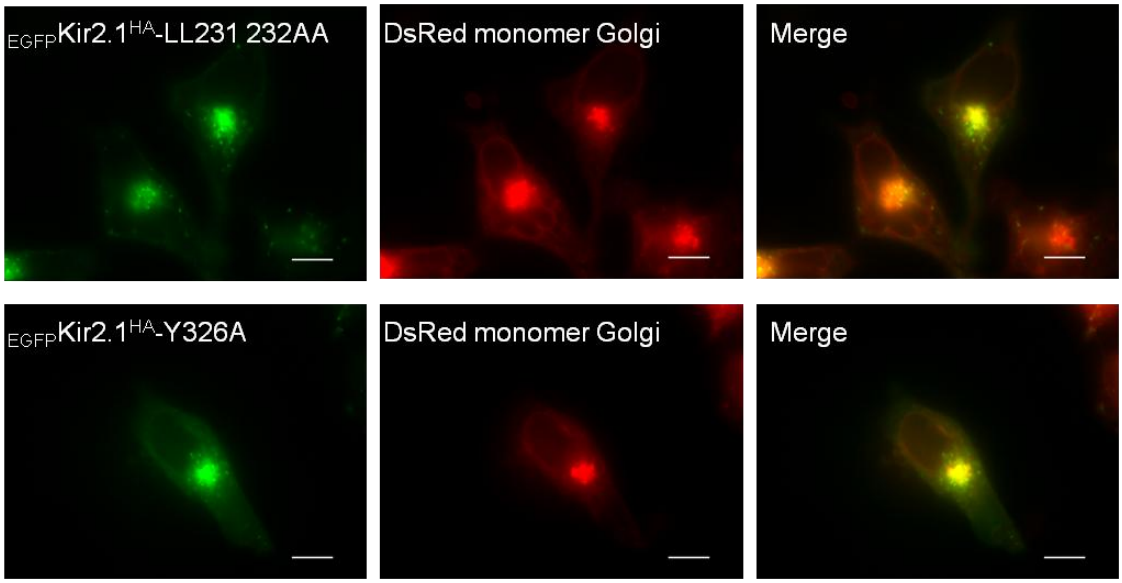

Figure 3.7 Subcellular localization of the Kir2.1 mutants ($_{EGFP}Kir2.1^{HA}$LL231 232AA and $_{EGFP}Kir2.1^{HA}$ Y326A). Live cell image of HeLa cells co-transfected $_{EGFP}Kir2.1^{HA}$ mutants (green) with the Golgi marker DsRed Monomer Golgi (red). $_{EGFP}Kir2.1^{HA}$ LL231232AA and $_{EGFP}Kir2.1^{HA}$ Y326A are co-localized together with Golgi marker DsRed monomer Golgi.

In contrast, the mutant LL231 232AA or Y326A was mainly localized to vesicular and perinuclear structures confirming the data obtained in our surface expression analysis (The mutant LL231 232AA or Y326A largely reduced the surface expression). The mutant LL231 232AA or Y326A co-labeled with the Golgi marker, DsRed Monomer Golgi, indicating the localization to the Golgi apparatus in HeLa cells (Figure 3.7).

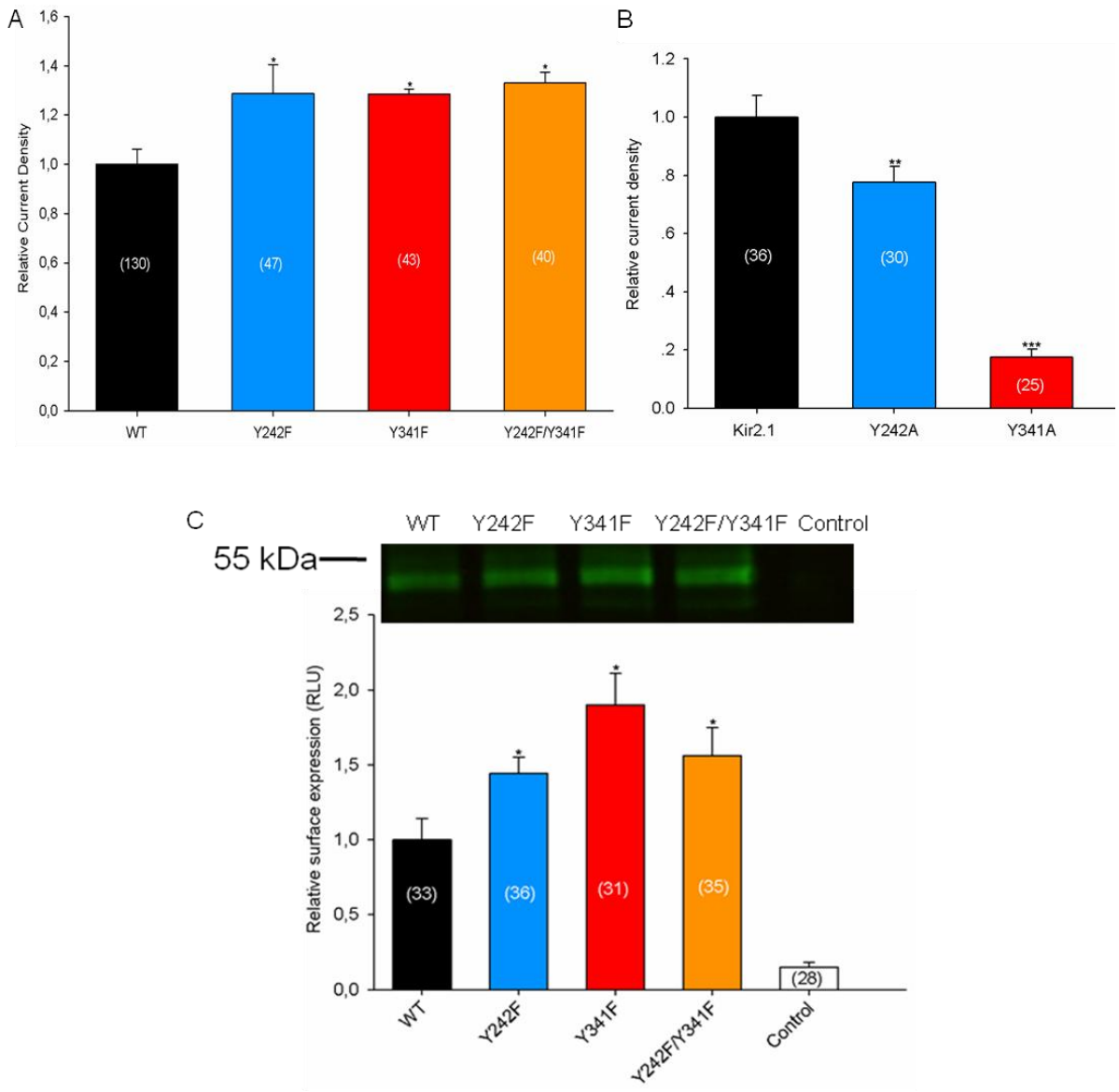

Figure 3.8 Identification of internalization signals in the C-terminal region of Kir2.1 channel in Xenopus oocytes. (A) The normalized inward current measured at -100 mV in Xenopus oocytes expressing Kir2.1 and conservative mutants. The number of oocytes is given in brackets. (B) The normalized inward current measured at -100 mV in Xenopus oocytes expressing Kir2.1 and two alanine mutations of ^{242}YIPL^{245} and ^{341}YSRF^{344}. The number of oocytes is given in brackets. (C) Surface expression of Kir2.1 and conservative mutants analyzed with a chemiluminescence assay in Xenopus oocytes. The number of oocytes is given in brackets. Inset: Western blot analysis of protein steady state levels of wild type and conservative mutants in Xenopus oocytes. Another independent experiment gave similar results.

To confirm the significant changes associated with the surface expression of the different endocytotic mutants, normalized inward current measured at -100 mV in Xenopus oocytes expressing Kir2.1 and mutants were quantified. The conservative mutants Y242F, Y341F and Y242F/Y341F significantly increased current density by 29%, 28% and 33% respectively compared to wild type Kir2.1 (Figure 3.8A). Surprisingly, the mutation Y242A significantly reduced current

density by 24% compared to wild type Kir2.1 channels. Finally, mutant Y341A also showed almost no or little currents (Figure 3.8B).

Additionally, surface expression of wild type Kir2.1 and the mutants was studied in Xenopus oocytes (Figure 3.8C). The conservative mutants Y242F, Y341F and Y242F/Y341F significantly increased surface expression by 44%, 90% and 56%, respectively, compared to wild type, indicating that the enhancement was likely the result of a change in channel trafficking. Western blots also confirmed approximately equal expression of all HA tag-Kir2.1 fusion protein in Xenopus oocytes (Figure 3.8C, inset). These data are in agreement with the data obtained by using COS-7 cells. Taken together, in mammalian cells as well as in Xenopus oocytes, disruption of the Y242 and Y341 motifs significantly increased the amount of Kir2.1 at cell surface.

3.4 Endocytic rate of WT, Y242A, Y341A and Y242A/Y341A

To visualize and quantify the internalization of Kir2.1 channels in COS-7 cells we performed an antibody uptake assay.

Figure 3.9A shows that wild type Kir2.1 channels have more internalized vesicles compared to the mutants Y242A, Y341A and Y241A/Y341A at different time points indicated by the higher number of red labeled vesicles. To quantify the endocytosis, the ratio of fluorescence intensity of internalized channels to fluorescence intensity of cell surface channels was determined. The cells were incubated at 37°C for 5, 10 or 15 min. The internalization rate of the mutants Y242A, Y341A or Y241A/Y341A was significantly reduced to 63%, 41% and 66% of control, respectively, compared to the wild type Kir2.1 channels (Figure 3.9B). The mutation Y341A had a larger effect on blocking endocytosis compared to the Y242A mutation. However, the internalization rate of double mutant Y242A/Y341A was similar to that of single mutant.

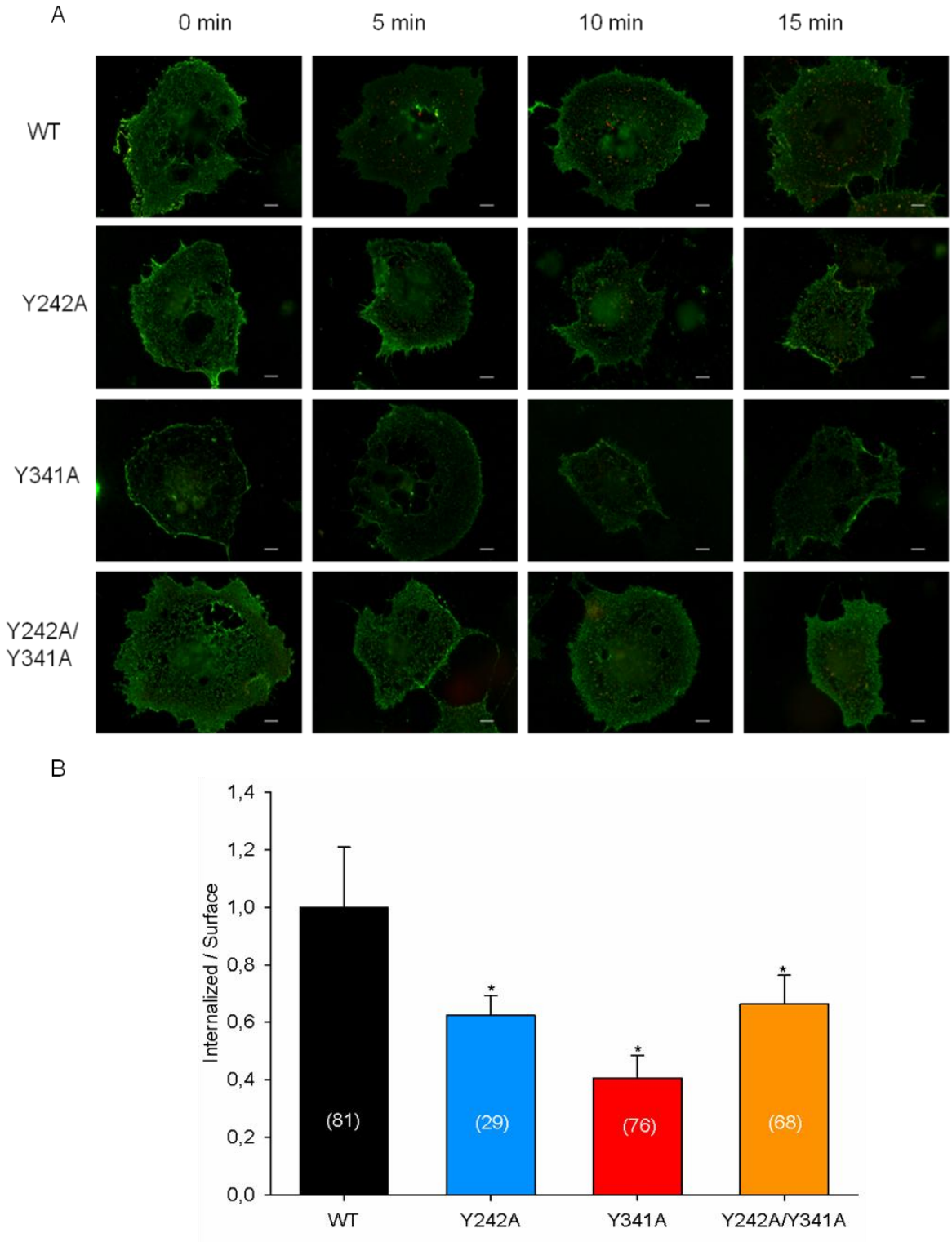

Figure 3.9 Quantification of wild type Kir2.1 channels and mutants using an antibody uptake assay. (A) COS-7 cells transfected with wild type Kir2.1 and mutants were analyzed for internalization (antibody uotake assay) as depicted in Figure 3.2B. Shown are representative fluorescent images of surface anti-HA (green) and internalized anti-HA (red) antibody at 0, 5, 10 and 15 min. Notably almost no internalization of wild type and mutants were detected at 0 min. Scale bar: 10 µm. (B) Quantification of wild type and mutants' endocytosis at 15 min. Data are expressed as the ratio of fluorescence intensity of internalized channels to fluorescence intensity of cell surface channels at the 15 minute. The number of cells for each condition is indicated in brackets. Significant differences from control wild type Kir2.1 were found (*P < 0.05) using the Student's t-test.

In order to confirm the above conclusions, and to further characterize the role of these novel endocytic motifs in trafficking, we measured the internalization of Kir2.1 and its mutants in HeLa cells using a biotinylation assay. The advantage of using this quantitative assay versus the fluorescent approach was that we could determine whether internalization was blocked (Figure 3.10A). Briefly, cell surface proteins were biotinylated under nonpermeabilized conditions at 4°C and then allowed to undergo endocytosis for a desired period of time at 37°C. Following internalization, cells were rapidly chilled on ice to stop the internalization process and surface biotinylated proteins were stripped off, internalized channels were detected by precipitation the cell lysates using NeutrAvidin agarose followed by Western blots with an anti-rat HA antibody. The stripping protocol was designed in a way to exclude the contamination from biotinylated proteins remaining on the surface.

The ratio of internalized channels to total channels was determined by densitometric analysis at 30 min chase time point on both wild type and mutants (n=4). As seen in Figure 3.10B, the internalization of the mutants Y242A, Y341A and Y242A/Y341A was significantly reduced by 49%, 27% and 43%, respectively, compared to wild type Kir2.1 channel. These results are consistent with the data obtained by the antibody uptake assay. In conclusion, it could be shown that the mutants Y242A, Y341A and Y242A/Y341A exhibit a decreased rate of internalization as compared to wild type Kir2.1 channels. These results also indicate that the increased surface expression presented in Figure 3.6 and Figure 3.8 is very likely due to a reduced endocytosis rate.

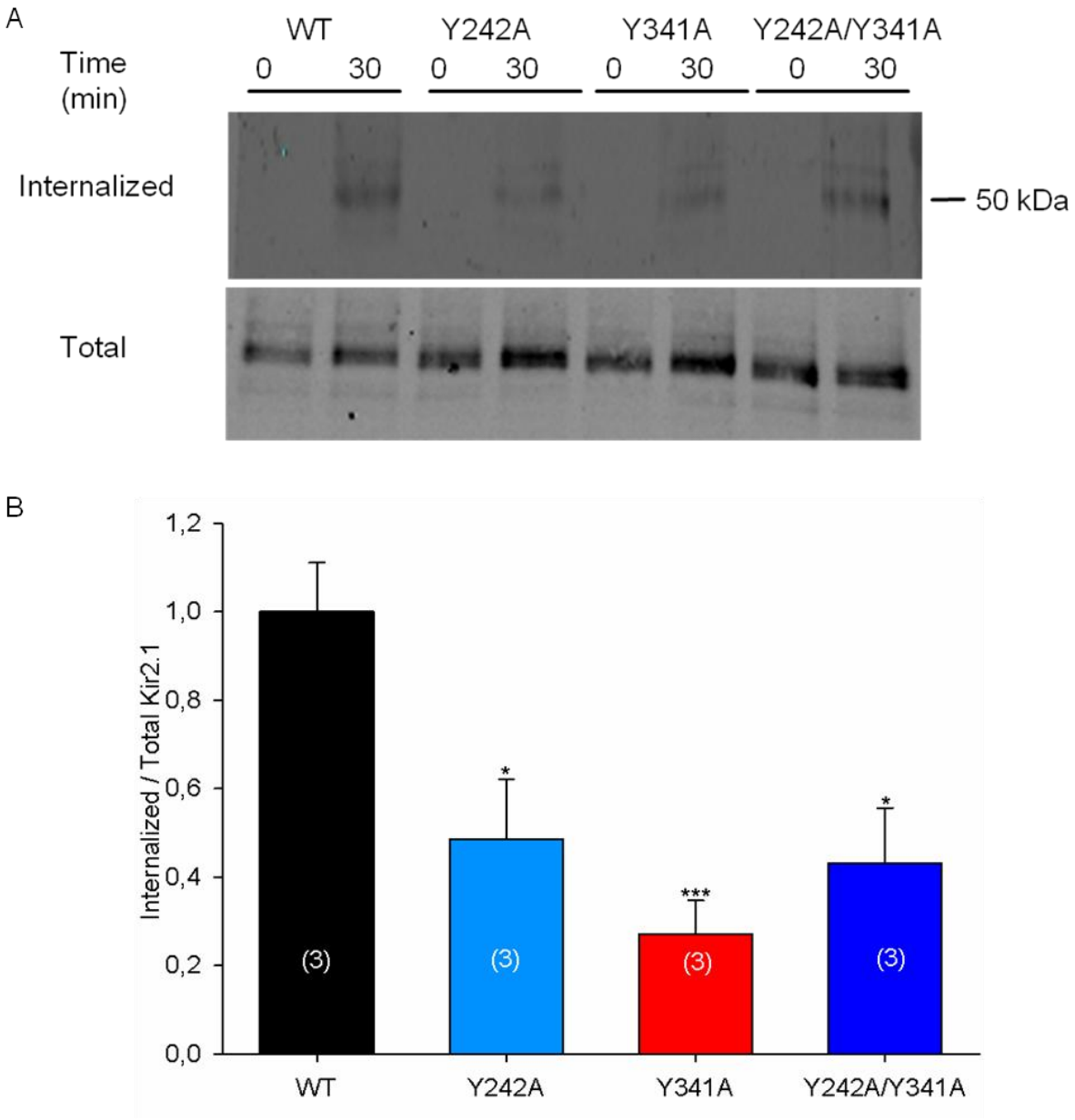

Figure 3.10 Quantification of wild type and mutants using a biotinylation internalization assay. (A) Comparison of the endocytosis rates of Kir2.1, Y242A, Y341A and Y242A/Y341A constructs. Cell surface biotinylation was performed using the non-permeable cleavable biotinylation reagent Sulfo-NHS-SS-Biotin (1 mg/ml) on wild type and mutants transfected cells and internalization was detected as described in Materials and methods. Representative western blots are shown detecting from left to right, strip control (0′, +strip) and internalization for 30 min (30′, +strip) for WT and mutants, using an anti-rat HA antibody. (B) Quantification of wild type and mutants endocytosis at 30 min. Data are expressed as the ratio of internalized channels to total channels by densitometry and presented as mean±SEM (n=3). The difference in internalization between wild type channel and its mutants was found to be statistically significant (*P < 0.01, ***P ＜0.001), using the Student's t-test.

3.5 The endocytotic signals from Kir2.1 channels are transplantable

The importance and role of each of the tyrosine residues for the internalization was further tested by using CD8 reporter assay. Classic trafficking signals of membrane proteins are often transplantable to other membrane proteins (Mason *et al.*, 2008; Ortega *et al.*, 2012). Previous research has showed that attaching the N- or C-terminal parts of Kir2.1 channel alone to the CD8 reporter protein resulted in Golgi accumulation of the fusion protein.

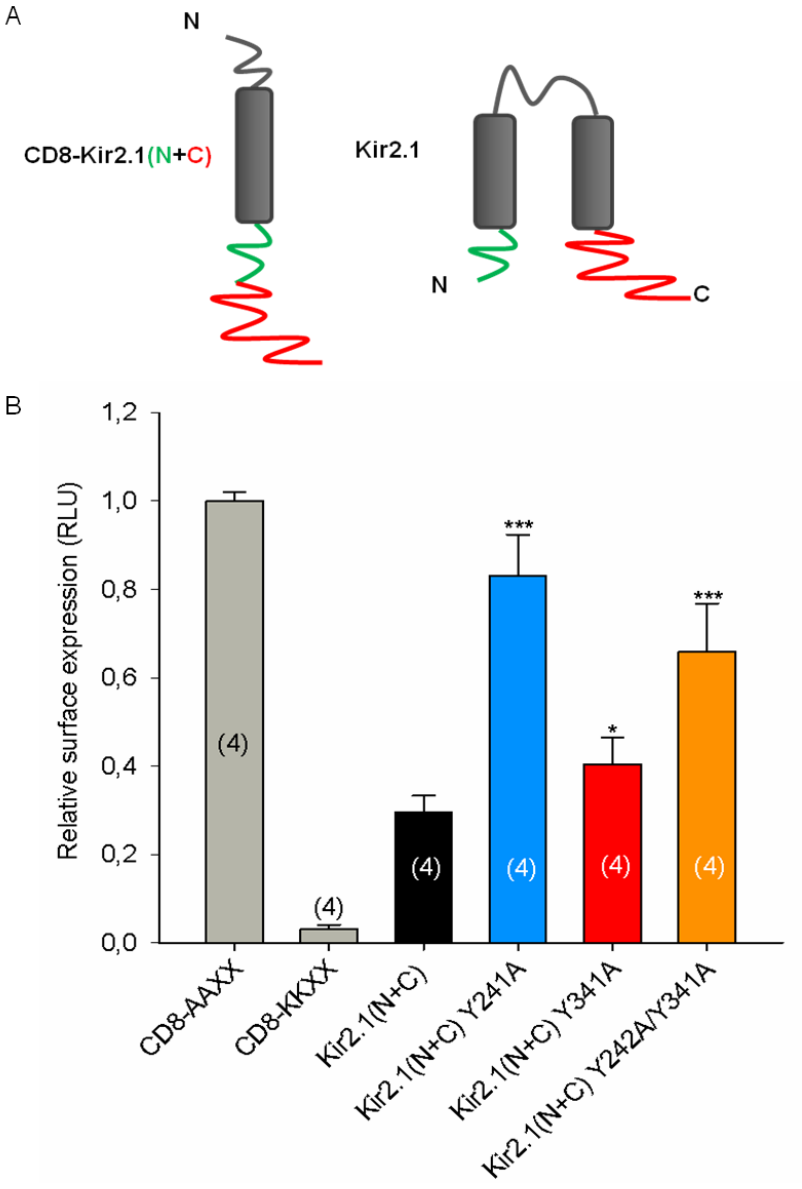

Figure 3.11 Quantification of surface expression of CD8 fusion constructs in COS-7 cells. (A) Cartoon of the CD8-Kir2.1 chimeras. CD8-Kir2.1 (N+C) is a fusion of CD8 extracellular and transmembrane domain with a Kir2.1 N-C cytoplasmic domain. (B) The surface expression of the mutants based on CD8-Kir2.1 (N+C) construct was compared to the surface expression of CD8-Kir2.1 (N+C). Results from four independent experiments were normalized to the values obtained for CD8-Kir2.1 (N+C). The ER retention motif KKXX served as a positive control for retention and AAXX as a negative control.

However, an artificial combination of the N-and C-terminal together fused to the CD8 reporter protein (Figure 3.11A) reached the cell surface efficiently (Ma *et al.*, 2011). Therefore, a chimeric CD8-Kir2.1 (N+C) construct was generated containing the extracellular and transmembrane domains of CD8 and a fusion of the N-terminal and C-terminal fragment of Kir2.1. To quantify the cell surface expression of these fusion constructs, we used a chemiluminescence assay. As shown in Figure 3.11B, the mutants Y242A, Y341A and Y242A/Y341A showed significant increase in surface expression by 181%, 37% and 122% respectively as compared to CD8-Kir2.1 (N+C). CD8-Kir2.1 chimeras demonstrate that the endocytosis signals from Kir2.1 channels are transplantable.

3.6 The endocytotic ^{242}YXXL^{245} and ^{341}YXXF^{344} motifs are highly conserved in the potassium channel family

To analyze the conservation of the endocytosis signals, the sequence of the C-terminal region of Kir2.1, Kir2.2, Kir2.3, Kir2.4, Kir2.5, Kir2.6, Kir6.1 and Kir6.2 channels from different species were aligned. Fully or partially conserved residues are shown in red (Figure 3.12A). Two endocytotic motifs, YIPL and YSRF, are highly conserved within Kir2.X channel and Kir6.X channel family. The endocytic motif, YIPL, is conserved in the Kir2.X channel of various species, but it is not found in Kir6.1 or Kir6.2 of various species. Another endocytic motif, YXXF, is highly conserved in the Kir2.X channel (except Kir2.6) and Kir6.X channel family (Figure 3.12B).

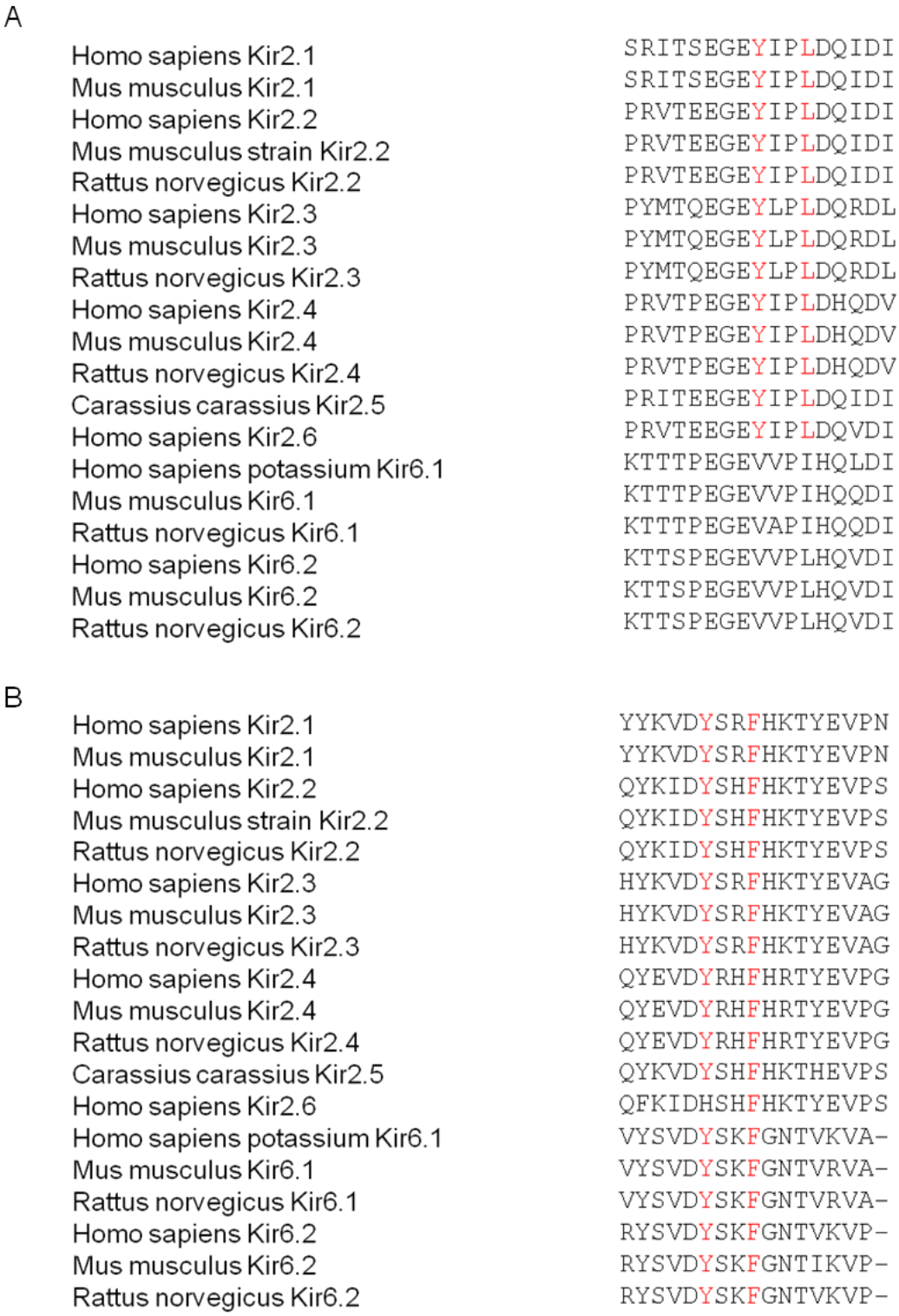

Figure 3.12 Sequence alignment of the C-terminal region of Kir2.1, Kir2.2, Kir2.3, Kir2.4, Kir2.5, Kir2.6, Kir6.1 and Kir6.2 with orthologous region from the different species. (A) YXXL endocytic motif identified in Kir2.1 is conserved in Kir2.X. (B) Another YXXF endocytic motif identified in Kir2.1 is highly conserved in Kir2.X (except Kir2.6) and Kir6.X.

We have shown that the mutation of Y341A in Kir2.1 channels lead to decreased endocytosis and increased surface expression. Next, we tested a comparable position ^{348}YSHF^{351} in Kir2.2 channels. To our surprise, analogues

mutant ^{348}ASHF^{351} in Kir2.2 had the opposite effect, it largely reduced cell surface expression (Figure 3.13A) and the majority of Kir2.2 channels were localized in an intracellular compartment (Figure 3.13B).

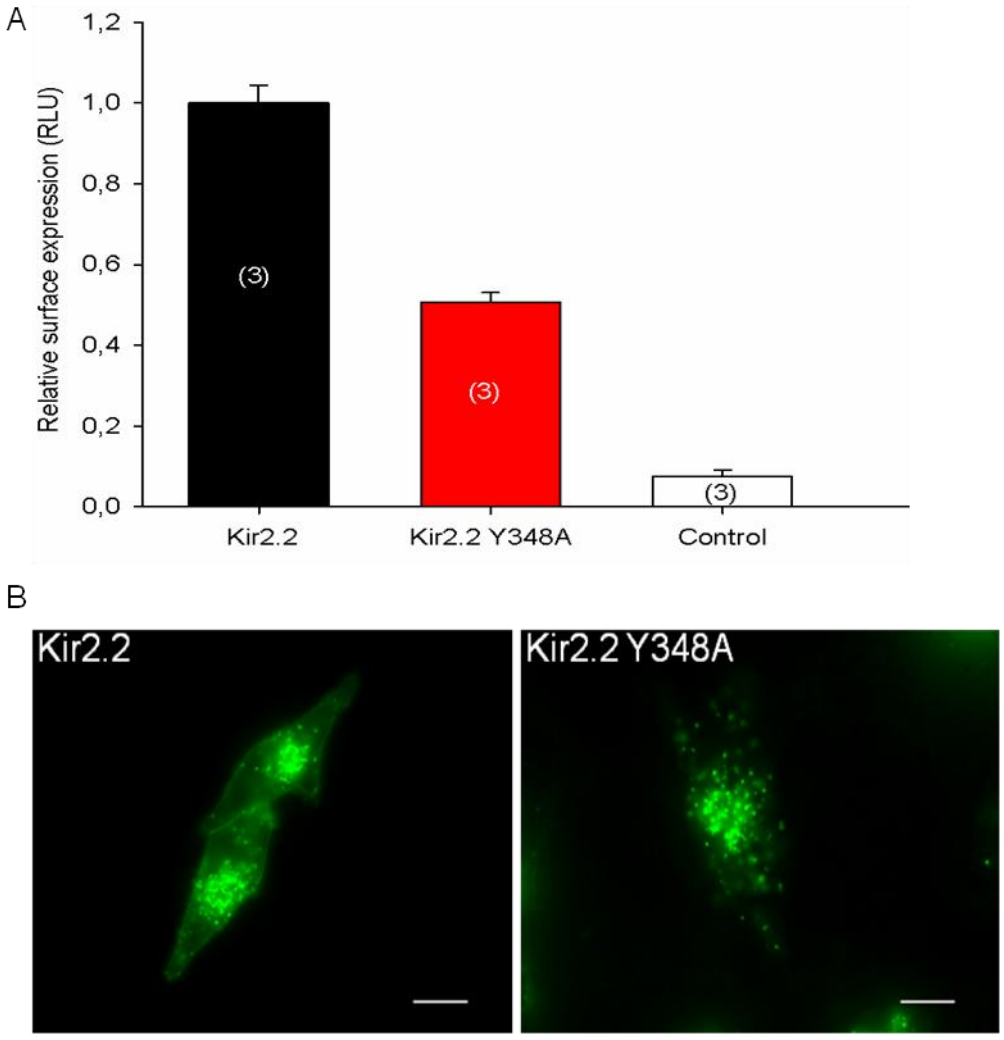

Figure 3.13 Analysis comparable putative endocytic motif ^{348}YSHF^{351} in Kir2.2 channel. (A) Point mutations of comparable putative endocytic motif ^{348}YSHF^{351} were introduced into the C-terminal domain of Kir2.2 channel. This mutant was expressed in COS-7 cells and surface expression was quantified using a chemiluminescence assay (see Materials and methods).The number of independent transfections is indicated in brackets. The value for the wild type channel was normalised to 1.0 and the mutant data expressed relative to wild type. (B) Representative live cell images of HeLa cells expressing $_{EGFP}$Kir2.2^{HA} constructs.

3.7 Kir2.1 is targeted to the endosome-lysosomal and endosomal-recycling pathway

To investigate which pathway Kir2.1 is targeted after internalization co-expression Kir2.1 with endosomal markers was performed and analyzed by fluorescence microscopy. Live cell imaging clearly showed that Kir2.1 channels strongly colocalized with the early endosomal marker, Rab5 or with the late late endosomal marker, Rab7. There was also some co-localisation with Lyso-Tracker Red (a red-fluorescent dye for labeling and tracking acidic organelles in live cells. The sub-cellular localization to endosome-lysosomal pathway is in agreement with the previous published results (Figure 3.14A, 3.14B, 3.15B) (Jansen *et al.*, 2008; Varkevisser *et al.*, 2013). We also found that Kir2.1 channels partially colocalized with the recycling endosomal marker, Rab11 (Figure 3.15A). These data suggest that Kir2.1 is targeted to the endosome-lysosomal and endosomal-recycling pathway.

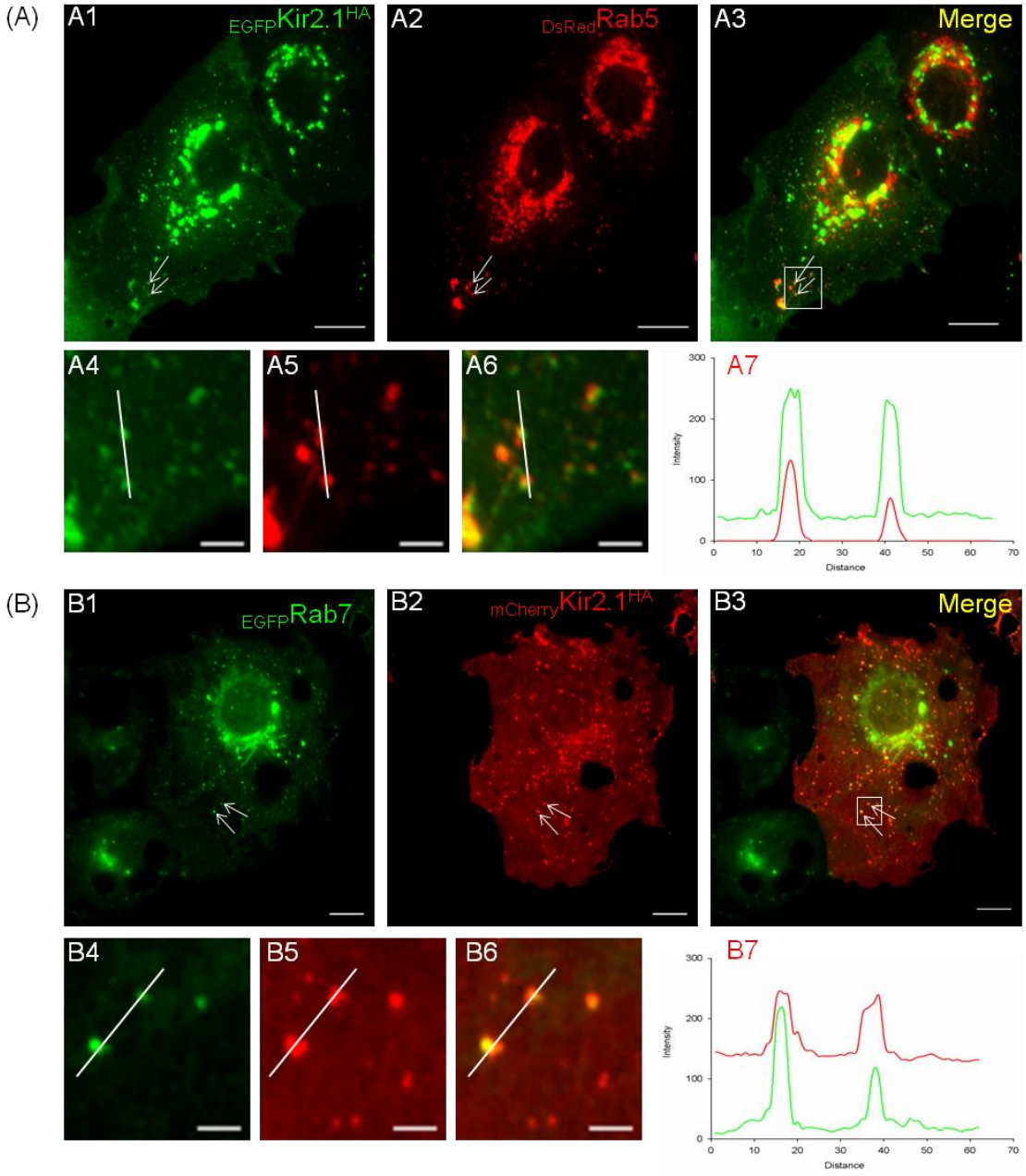

Figure 3.14 Live-cell imaging of HeLa cells co-transfected with fluorescence-labeled Kir2.1 and the endosomal markers fluorescence-labeled Rab5 and Rab7. (A) Colocalization of $_{EGFP}Kir2.1^{HA}$ and DsRedRab5. (B) Colocalization of $_{mCherry}Kir2.1^{HA}$ and $_{EGFP}$Rab7. (A4-B4) and (A5-B5) represented higher magnifications of the regions indicated by the arrows in (A3-B3). (A7-B7) were intensity profiles of (A6-B6). All images were taken 24 h or 48 h after transfection. Similar results were obtained in at least three times transfections. Scale bars, 10 µm.

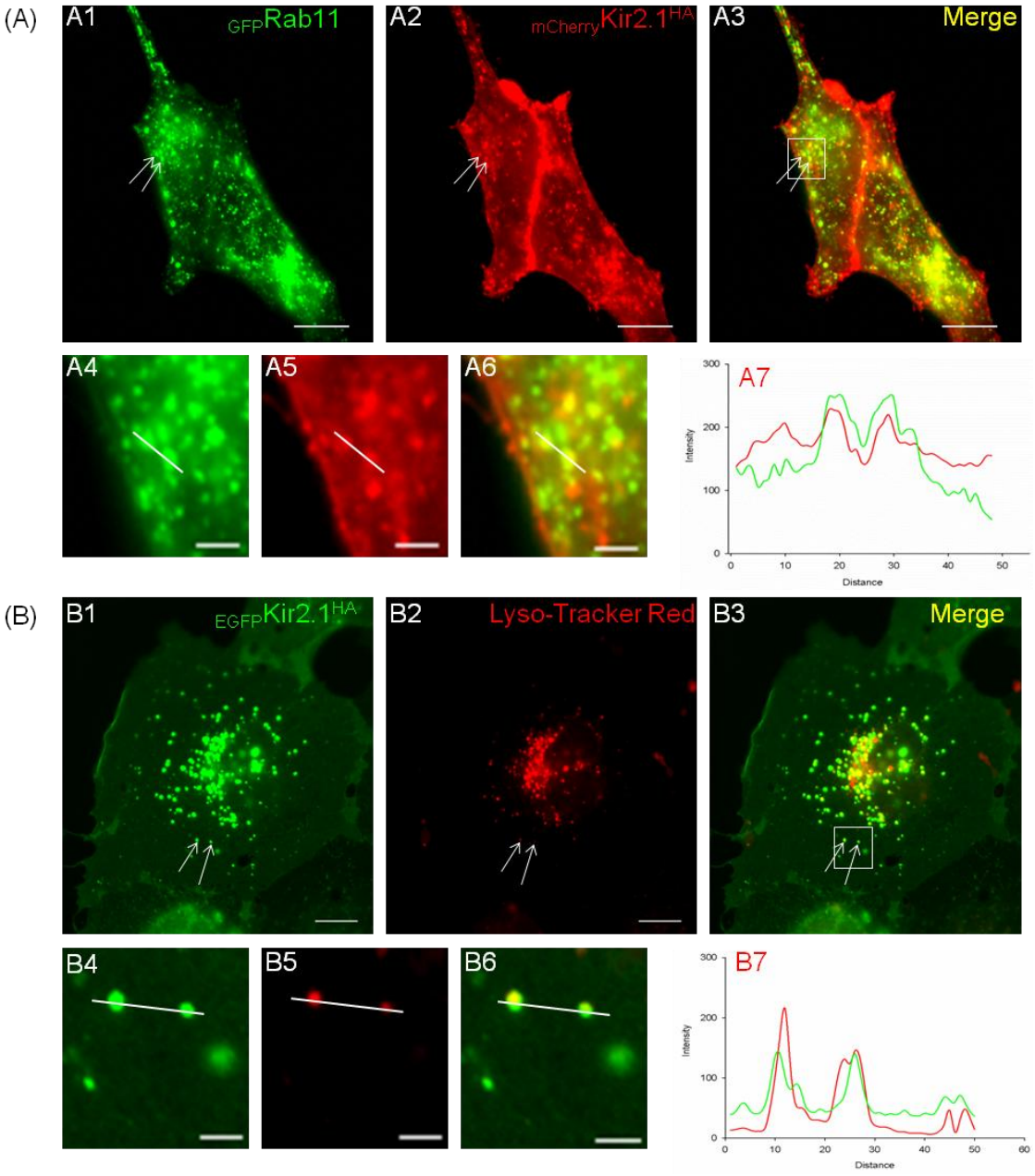

Figure 3.15 Live-cell imaging of HeLa cells co-transfected with fluorescence-labeled Kir2.1 and the endosomal markers fluorescence-labeled Rab11 and Lysosome staining (Lyso-Tracker Red). (A) Colocalization of $_{mCherry}Kir2.1^{HA}$ and $_{EGFP}Rab11$. (B) Colocalization of $_{EGFP}Kir2.1^{HA}$ and Lyso-Tracker Red (treated with lysosome inhibitor, Leupeptin 10 μm, overnight, and then stained with Lyso-Tracker Red). (A4-B4) and (A5-B5) represented higher magnifications of the regions indicated by the arrows in (A3-B3). (A7-B7) were intensity profiles of (A6-B6). All images were taken 24 h or 48 h after transfection. Similar results were obtained in at least three times transfections. Scale bars, 10 μm.

4. Discussion

The potassium channel Kir2.1, a strong inward rectifier, is functionally important in many cell types including neurons and cardiac muscle. Thus, regulating Kir2.1 channel activity would influence the electrophysiology of such cells. The channel activity can be regulated by two ways, which is either by changing the open probability or by changing the number of channels at the cell membrane. The cell surface expression, in turn, is regulated by the forward trafficking of the channel or its endocytosis from the membrane. However, the cytoplasmic signals that regulate the internalization of Kir2.1 channels are still poorly understood. In this study we examined the cellular mechanisms controlling the endocytosis of Kir2.1. Our major new results are (i) We show that Kir2.1 undergoes constitutive internalization (Figure 3.2); (ii) We show that Kir2.1 is internalized via a clathrin and dynamin dependent pathway (Figure 3.3); (iii) We characterized two novel tyrosine based endocytic motifs ^{242}YIPL^{245} and ^{341}YSRF^{344} in the C-terminal domain of Kir2.1 (Figure 3.6, Figure 3.8); (iv) We show that Kir2.1 can be transported along Rab5-Rab11 recycling pathway and along the endosome-lysosome protein degradation pathway (Figure 3.14 and Figure 3.15).

So far, several modes of endocytosis have been described in the past, including clathrin dependent endocytosis, caveolin dependent endocytosis, clathrin and caveolin independent endocytosis (McMahon and Boucrot, 2011). Several lines of evidence demonstrate that Kir2.1 is internalized by clathrin and dynamin mediated endocytosis. Co-expression of a dominant-negative mutant of dynamin (K44A), but not wild-type dynamin, strongly enhanced the surface expression of Kir2.1 (Figure 3.3A). Similarly, the C-terminal part of the adapter protein AP180 (AP180C) increased the cell surface expression of Kir2.1 though inhibition of endocytosis (Figure 3.3B and 3.3C), which are consistent with previous research (Groves *et al.*, 2007; Varkevisser *et al.*, 2013). Moreover, immunprecipitation experiments have also shown that Kir2.1 interacts with the µ-2 subunit of the AP2 complexes in vitro (Figure 3.4).

There are four tyrosine based ^{242}YIPL^{245}, ^{326}YEPV^{329}, ^{336}YYKV^{339}, ^{341}YSRF^{344} and a dileucine-based ^{228}RAQLL^{232} potential endocytic motifs in the C-terminal domain of Kir2.1 channel. However, only two mutations of ^{242}YIPL^{245} and

^{341}YSRF^{344} inhibited internalization. Based on recently solved crystal structure of Kir2.1, it seems plausible that these two motifs ^{242}YIPL^{245} and ^{341}YSRF^{344} are solvent exposed, and could potentially bind AP2 complexes. In contrast, the motifs ^{228}RAQLL^{232}, ^{326}YEPV^{329} and ^{336}YYKV^{339} are buried and are unable to bind AP2 complexes. This explains why mutations ^{228}RAQLL^{232}, ^{326}YEPV^{329} and ^{336}YYKV^{339} have no effect on Kir2.1 endocytosis. In addition to the motifs that we characterized here, there is one more potential tyrosine based endocytic motif ^{9}YSIV^{12} in the N terminal region of Kir2.1. However, Mason, A. et.al reported that this motif is not involved in the endocytosis of Kir2.1 channels (Mason, 2008).

The two tyrosine based endocytic motifs analyzed here, ^{242}YXXL^{245} and ^{341}YXXF^{344}, are well conserved in all Kir2.X and Kir6.X channel family members, raising the possibility that this motifs might serve as a general endocytic motifs for these carriers. One of these endocytic motifs ^{242}YXXL^{245} is conserved in the Kir2.X channel of various species, but it is not found in Kir6.1 or Kir6.2 of various species (Figure 3.12A). Another endocytic motif ^{341}YXXF^{344} is highly conserved in the Kir2.X channel (except Kir2.6) and Kir6.X channel family members (Figure 3.12B). These observations suggest a mechanism controlling the endocytosis of Kir2.X and Kir6.X family members may be conserved.

Tong et al., reported that phosphorylation of tyrosine 242 of Kir2.1 may in some way or other stimulate the rate of endocytosis of Kir2.1 (Tong *et al.*, 2001). In contrast, we show that in both Xenopus oocytes and mammalian cell lines the motif ^{242}YIPL^{245} is involved in clathrin mediated endocytosis without any requirement for tyrosine phosphorylation. Notably, the motif ^{341}YSRF^{344} may play a much more prominent role in Kir2.1 endocytosis because the mutation of this motif had stronger effects compared to the mutation of ^{242}YIPL^{245} on blocking endocytosis. Additionally, we tested a homologous motif ^{348}YSHF^{351} in Kir2.2 channels on its effect on endocytosis. Surprisingly, the mutant ^{348}ASHF^{351} in Kir2.2 channels had the opposite effect, largely reduced cell surface expression (Figure 3.13A) and the majority of Kir2.2 was localized to an intracellular compartment (Figure 3.13B). Interestingly, a di-hydrophobic signal ^{413}II^{414} not a homologous and conserved motif ^{332}YSRF^{335} in Kir2.3 channel has been reported to be responsible for mediating endocytosis (Mason *et al.*, 2008;

Ortega *et al.*, 2012). The difference may be related to different physiological functions Kir2.1 versus Kir2.2 and Kir2.3 (Scherer *et al.*, 2007; Mason, 2008; Zhao *et al.*, 2008; Boyer *et al.*, 2009; Seebohm *et al.*, 2012; Liang *et al.*, 2014). However, another comparable position ^{330}YSKF^{333} in Kir6.2 channel has been reported to contribute to internalization (Sierra *et al.*, 2013).

Several groups have found that protein kinase and phosphatase inhibitors could influence Kir2.1 currents via the phosphorylation state of Y242 of Kir2.1 (Wischmeyer *et al.*, 1998; Gao *et al.*, 2004; Sun *et al.*, 2007; Hinard *et al.*, 2008; Zhao *et al.*, 2008). Another study suggested that the phosphorylation or de-phosphorylation of Y242 of Kir2.1 may influence clathrin dependent endocytosis of Kir2.1 (Tong *et al.*, 2001). Indeed, our results and previous research support a model in which clathrin-dependent internalization is induced via de-phosphorylation of the tyrosine residue Y242 in the C-terminal tail of Kir2.1.

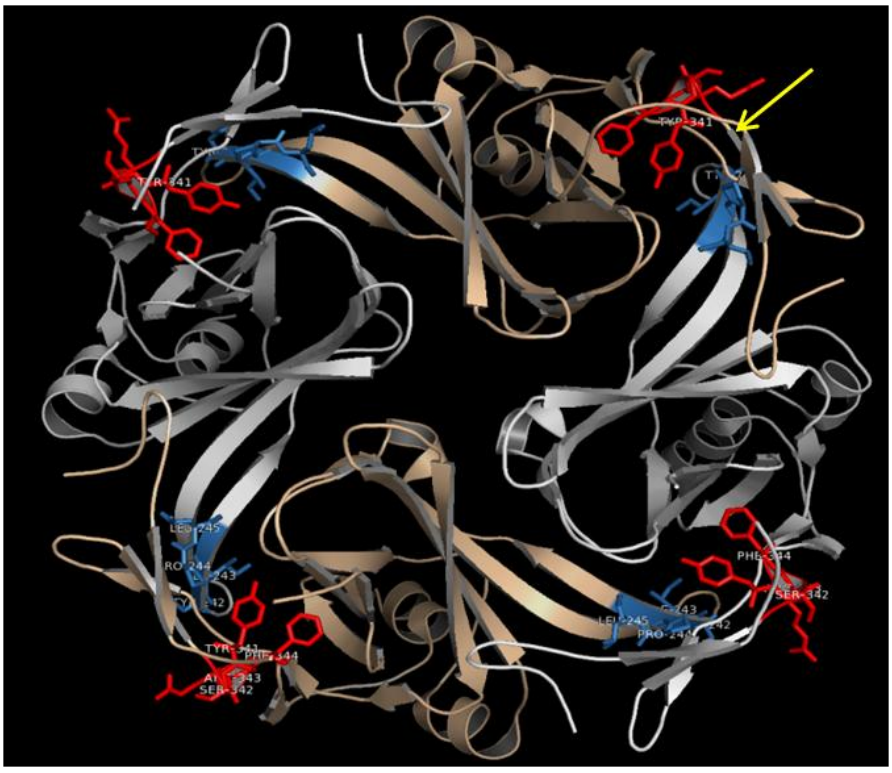

Figure 4.1 The image depicts the location of the two functional endocytic motifs ^{242}YIPL^{245} and ^{341}YSRF^{344} in the 3D structure determined for the cytoplasmic domain of the Kir2.1 channel. ^{242}YIPL^{245} motifs are illustrated in blue. ^{341}YSRF^{344} motifs are illustrated in red. The cytosolic pore viewed from the top (membrane to cytoplasm), modified from Pegan et al., 2005.

The signals driving clathrin-mediated endocytosis in the Kir channel family are diverse and include YXXΦ type motifs, NPXY type motifs, di-leucine (LL) type signals and di- leucine (II) type signals (Tong *et al.*, 2001; Zeng *et al.*, 2002; Hu

et al., 2003; Mason *et al.*, 2008; Fang *et al.*, 2009; Ortega *et al.*, 2012; Sierra *et al.*, 2013). Multiple endocytosis signals may be involved to regulate membrane proteins trafficking (Sunder‐Plassmann *et al.*, 1997; HU *et al.*, 2001; Lu *et al.*, 2002; Kinlough *et al.*, 2004; Pandey *et al.*, 2008; Xu *et al.*, 2009). For example, in the Kir6.2 channel, two endocytosis signals have been reported to mediate internalization (Hu *et al.*, 2003; Sierra *et al.*, 2013). In our study, we showed that two YXXΦ-based endocytic motifs ^{242}YIPL^{245} and ^{341}YSRF^{344} may enhance the surface expression of Kir2.1. This effect is most likely attributable to a decrease in endocytosis, therefore it appears that both tyrosine based motifs ^{242}YIPL^{245} and ^{341}YSRF^{344} may be responsible for endocytosis. If in this case, we would expect to see an addictive effect of double mutation ^{242}YIPL^{245} and ^{341}YSRF^{344}. However, surprisingly, with all experimental approaches employed, mutating both tyrosine residues had the similar effect as mutating either one of them (Figure 3.6B, 3.6C, 3.8A, 3.8C, 3.9 and 3.10). These results raise the possibility that AP2 may simultaneously bind two endocytic motifs. The simplest explanation for our results suggest is that both motifs ^{242}YIPL^{245} and ^{341}YSRF^{344} may create a ‘signal patch’ (Figure 4.1, yellow arrow), which could bind to the same AP-2 complex simultaneously and promote endocytosis in a co-operative manner (Figure 4.1). Indeed the two endocytosis signals studies here are localised in close vicinity in the assembled tetrameric channel. Thus, the endocytosis of Kir2.1 channels may require both endocytosis signals to be present for endocytosis to occur. In other words, AP-2 may bind to Kir2.1 channels with a much higher 'avidity' when both endocytosis signals are present. Thus, efficient endocytosis may depend on a coincidence detection mechanism of the adaptor protein AP-2. The structural motif of both endocytosis signals exposed in close vicinity may represent a quality control mechanism that couples protein conformation to endocytosis, similar to the case of Golgi export mediated by the adaptor protein AP-1 (Ma *et al.*, 2011). Further studies are needed to determine whether the motifs ^{242}YIPL^{245} and ^{341}YSRF^{344} indeed bind directly and simultaneously to the AP2 complex.

The structural model described here (Figure .4.1) may also be useful for understanding the differences observed when we replaced the tyrosine residue in the YSRF motif by alanine or by the more similar phenylalanine. The mutated motif ^{341}ASRF^{344} in Kir2.1 channel resulted in a non-functional channel that

conducted almost no current (Figure 3.8B), whereas the conservative mutant ^{341}FSRF^{344} resulted in a functional channel. Furthermore, the conservative and functional mutant ^{341}FSRF^{344} produced much more current compared to wild type Kir2.1 (Figure 3.8A), most likely by increasing the cell surface expression of the channel compared to wild type Kir2.1 (Figure 3.8C). As an explanation, the mutation ^{341}ASRF^{344} in Kir2.1 might result in a conformational change that disturbed the tertiary structure of the 'inner pore' of the channel, whereas the tertiary structure may be conserved after replacement of tyrosine by phenylalanine. This may be the reason why the ASRF mutants produced very little current when expressed in Xenopus oocytes. The same explanation may apply for the ^{242}AIPL^{245} mutation, which was also associated with a decreased Kir2.1 current compared to wild type Kir2.1 (Figure 3.8B) while the conservative mutation ^{242}FIPL^{245} produced more current than wild type Kir2.1 (Figure 3.8A). Again, probably the mutation ^{242} AIPL^{245} changed the conformation of Kir2.1 compared to the conservative mutation ^{242}FIPL^{245} more dramatically, resulting in a channel with a lower open probability. In conclusion, the simplest explanation for our results is that the ASRF and AIPL mutants were associated with impaired endocytosis (increased surface expression) and at the same time with a reduced Kir2.1 current (change in tertiary structure), whereas the FSRF and FIPL mutants were only associated with an impaired endocytosis (Figure. 3).

Several previous studies have shown that Kir2.1 is targeted to the lysosomal degradation pathway (Jansen *et al.*, 2008; Varkevisser *et al.*, 2013). We have confirmed this in our present study (Figure 3.14A, 3.14B, 3.15B). Additionally, we obtained some evidence that Kir2.1 may also be targeted to endosomal-recycling pathway (Figure 3.15A).

In conclusion, two endocytic motifs ^{242}YIPL^{245} and ^{341}YSRF^{344} identified in this study regulate the constitutive clathrin-mediated endocytosis of Kir2.1.

Summary

We have studied some of the mechanisms responsible for controlling the density of Kir2.1 channels at the cell surface. In particular, we have explored the mechanisms underlying the of Kir2.1 channel into the endocytic pathway. We found that

1. The antibody uptake assay showed that about 20% of the antibodies labeled surface channels were internalized within 5 min of temperature shift; an apparent maximum was reached after 15 min. Kir2.1 undergoes constitutive internalization.

2. Co-expression of a dominant-negative mutant of dynamin K44A or AP180C enhanced the surface expression of Kir2.1 by 40% and 49% respectively. AP180C inhibited clathrin mediated internalization of Kir2.1 by 80% compared with COS-7 cells transfected with Kir2.1 and a control vector. Kir2.1 is internalized by clathrin-mediated endocytosis.

3. In both Xenopus oocytes and mammalian cells system, disruption of Y242 and Y341 motif significantly increased the amount of Kir2.1 at cell surface respectively. The mutants Y242A and Y341A also showed dramatic decrease in the rate of endocytosis as compared to wild-type Kir2.1 channels respectively. Two tyrosine based endocytic motifs ^{242}YIPL^{245} and ^{341}YSRF^{344} in the C-terminal domain of Kir2.1 are both involved in the endocytosis of Kir2.1.

4. Live cell imaging clearly showed that Kir2.1 channels strongly colocalized with early endosomal marker, Rab5 or late endosomal marker, Rab7 or recycling endosome marker, Rab11 or Lyso-Tracker Red. Kir2.1 is targeted to the endosome-lysosomal and endosomal- recycling pathway.

5. The two endocytosis signals studied here are in close vicinity as indicated by the tertiary structure of the cytosolic pore of Kir2.1 channels. Since mutation of both motifs had the similar effect as mutation of only one of these motifs. We hypothesize that both signals must be present for efficient constitutive endocyosis to occur.

References

Abraham MR, JAHANGIR A, ALEKSEEV AE & TERZIC A. (1999). Channelopathies of inwardly rectifying potassium channels. *The FASEB journal* 13, 1901-1910.

Anumonwo JM & Lopatin AN. (2010). Cardiac strong inward rectifier potassium channels. *J Mol Cell Cardiol* 48, 45-54.

Bonifacino JS & Traub LM. (2003). Signals for Sorting of Transmembrane Proteins to Endosomes and Lysosomes*. *Annual review of biochemistry* 72, 395-447.

Boyer SB, Slesinger PA & Jones SV. (2009). Regulation of Kir2.1 channels by the Rho-GTPase, Rac1. *Journal of cellular physiology* 218, 385-393.

De Boer T, Houtman M, Compier M & Van der Heyden M. (2010). The mammalian KIR2. x inward rectifier ion channel family: expression pattern and pathophysiology. *Acta Physiologica* 199, 243-256.

Doherty GJ & McMahon HT. (2009). Mechanisms of endocytosis. *Annual review of biochemistry* 78, 857-902.

Doyle DA, Cabral JM, Pfuetzner RA, Kuo A, Gulbis JM, Cohen SL, Chait BT & MacKinnon R. (1998). The structure of the potassium channel: molecular basis of K+ conduction and selectivity. *science* 280, 69-77.

Fang L, Garuti R, Kim B-Y, Wade JB & Welling PA. (2009). The ARH adaptor protein regulates endocytosis of the ROMK potassium secretory channel in mouse kidney. *The Journal of clinical investigation* 119, 3278-3289.

Gao Z, Lau C-P, Wong T-M & Li G-R. (2004). Protein tyrosine kinase-dependent modulation of voltage-dependent potassium channels by genistein in rat cardiac ventricular myocytes. *Cellular signalling* 16, 333-341.

Giovannardi S, Forlani G, Balestrini M, Bossi E, Tonini R, Sturani E, Peres A & Zippel R. (2002). Modulation of the inward rectifier potassium channel IRK1 by the Ras signaling pathway. *Journal of Biological Chemistry* 277, 12158-12163.

Grant B & Sato M. (2006). Intracellular trafficking (January 21, 2006), WormBook, ed. The C. elegans Research Community, WormBook, doi/10.1895/wormbook. 1.77. 1.

Groves B, Gong Q, Xu Z, Huntsman C, Nguyen C, Li D & Ma D. (2007). A specific role of AGS3 in the surface expression of plasma membrane proteins. *Proceedings of the National Academy of Sciences* 104, 18103-18108.

Heginbotham L, Lu Z, Abramson T & MacKinnon R. (1994). Mutations in the K+ channel signature sequence. *Biophysical Journal* 66, 1061-1067.

Hibino H, Inanobe A, Furutani K, Murakami S, Findlay I & Kurachi Y. (2010). Inwardly rectifying potassium channels: their structure, function, and physiological roles. *Physiological reviews* 90, 291-366.

Hinard V, Belin D, Konig S, Bader CR & Bernheim L. (2008). Initiation of human myoblast differentiation via dephosphorylation of Kir2. 1 K+ channels at tyrosine 242. *Development* 135, 859-867.

Ho K, Nichols CG, Lederer WJ, Lytton J, Vassilev PM, Kanazirska MV & Hebert SC. (1993). Cloning and expression of an inwardly rectifying ATP-regulated potassium channel.

Hofherr A, Fakler B & Klöcker N. (2005). Selective Golgi export of Kir2. 1 controls the stoichiometry of functional Kir2. x channel heteromers. *Journal of cell science* 118, 1935-1943.

Hu K, Huang CS, Jan YN & Jan LY. (2003). ATP-sensitive potassium channel traffic regulation by adenosine and protein kinase C. *Neuron* 38, 417-432.

HU W, HOWARD M & Lukacs G. (2001). Multiple endocytic signals in the C-terminal tail of the cystic fibrosis transmembrane conductance regulator. *Biochem J* 354, 561-572.

Jansen JA, de Boer TP, Wolswinkel R, van Veen TA, Vos MA, van Rijen HV & van der Heyden MA. (2008). Lysosome mediated Kir2. 1 breakdown directly influences inward rectifier current density. *Biochemical and biophysical research communications* 367, 687-692.

Jones SP. (2003). Role of the small GTPase Rho in modulation of the inwardly rectifying potassium channel Kir2. 1. *Molecular Pharmacology* 64, 987-993.

Katz B. (1949). * LES CONSTANTES ELECTRIQUES DE LA MEMBRANE DU MUSCLE. *Archives des Sciences physiologiques* 3, 285-300.

Kinlough CL, Poland PA, Bruns JB, Harkleroad KL & Hughey RP. (2004). MUC1 membrane trafficking is modulated by multiple interactions. *Journal of Biological Chemistry* 279, 53071-53077.

Kubo Y, Baldwin TJ, Jan YN & Jan LY. (1993). Primary structure and functional expression of a mouse inward rectifier potassium channel. *Nature* 362, 127-133.

Leonoudakis D, Conti LR, Radeke CM, McGuire LM & Vandenberg CA. (2004). A multiprotein trafficking complex composed of SAP97, CASK, Veli, and Mint1 is associated with inward rectifier Kir2 potassium channels. *The Journal of biological chemistry* 279, 19051-19063.

Leyland ML & Dart C. (2004). An alternatively spliced isoform of PSD-93/chapsyn 110 binds to the inwardly rectifying potassium channel, Kir2.1. *The Journal of biological chemistry* 279, 43427-43436.

Liang S, Wang Q, Zhang W, Zhang H, Tan S, Ahmed A & Gu Y. (2014). Carbon monoxide inhibits inward rectifier potassium channels in cardiomyocytes. *Nature communications* 5.

Lu J-C, Scott P, Strous GJ & Schuler LA. (2002). Multiple internalization motifs differentially used by prolactin receptor isoforms mediate similar endocytic pathways. *Molecular Endocrinology* 16, 2515-2527.

Ma D, Taneja TK, Hagen BM, Kim B-Y, Ortega B, Lederer WJ & Welling PA. (2011). Golgi export of the Kir2. 1 channel is driven by a trafficking signal located within its tertiary structure. *Cell* 145, 1102-1115.

Margeta-Mitrovic M. (2002). Assembly-dependent trafficking assays in the detection of receptor–receptor interactions. *Methods* 27, 311-317.

Mason AK. (2008). *Molecular mechanisms of endocytic and post-endocytic trafficking regulating Kir2. x channels*. ProQuest.

Mason AK, Jacobs BE & Welling PA. (2008). AP-2-dependent internalization of potassium channel Kir2. 3 is driven by a novel di-hydrophobic signal. *Journal of Biological Chemistry* 283, 5973-5984.

McMahon HT & Boucrot E. (2011). Molecular mechanism and physiological functions of clathrin-mediated endocytosis. *Nature reviews Molecular cell biology* 12, 517-533.

Nichols C & Lopatin A. (1997). Inward rectifier potassium channels. *Annual Review of Physiology* 59, 171-191.

Ortega B, Mason AK & Welling PA. (2012). A Tandem Di-hydrophobic Motif Mediates Clathrin-dependent Endocytosis via Direct Binding to the AP-2 ασ2 Subunits. *Journal of Biological Chemistry* 287, 26867-26875.

Pandey MS, Harris EN, Weigel JA & Weigel PH. (2008). The cytoplasmic domain of the hyaluronan receptor for endocytosis (HARE) contains multiple endocytic motifs targeting coated pit-mediated internalization. *Journal of Biological Chemistry* 283, 21453-21461.

Pegan S, Arrabit C, Zhou W, Kwiatkowski W, Collins A, Slesinger PA & Choe S. (2005). Cytoplasmic domain structures of Kir2.1 and Kir3.1 show sites for modulating gating and rectification. *Nature neuroscience* 8, 279-287.

Preisig-Muller R, Schlichthorl G, Goerge T, Heinen S, Bruggemann A, Rajan S, Derst C, Veh RW & Daut J. (2002). Heteromerization of Kir2.x potassium channels contributes to the phenotype of Andersen's syndrome. *Proceedings of the National Academy of Sciences of the United States of America* 99, 7774-7779.

Sandoz G & Levitz J. (2013). Optogenetic techniques for the study of native potassium channels. *Frontiers in molecular neuroscience* 6, 6.

Scherer D, Kiesecker C, Kulzer M, Günth M, Scholz EP, Kathöfer S, Thomas D, Maurer M, Kreuzer J & Bauer A. (2007). Activation of inwardly rectifying Kir2. x potassium channels by β3-adrenoceptors is mediated via different signaling pathways with a predominant role of PKC for Kir2. 1 and of PKA for Kir2. 2. *Naunyn-Schmiedeberg's archives of pharmacology* 375, 311-322.

Seebohm G, Strutz-Seebohm N, Ursu ON, Preisig-Müller R, Zuzarte M, Hill EV, Kienitz M-C, Bendahhou S, Fauler M & Tapken D. (2012). Altered stress stimulation of inward rectifier potassium channels in Andersen-Tawil syndrome. *The FASEB Journal* 26, 513-522.

Shieh C-C, Coghlan M, Sullivan JP & Gopalakrishnan M. (2000). Potassium channels: molecular defects, diseases, and therapeutic opportunities. *Pharmacological Reviews* 52, 557-594.

Sierra A, Zhu Z, Sapay N, Sharotri V, Kline CF, Luczak ED, Subbotina E, Sivaprasadarao A, Snyder PM & Mohler PJ. (2013). Regulation of cardiac ATP-sensitive potassium channel surface expression by calcium/calmodulin-dependent protein kinase II. *Journal of Biological Chemistry* 288, 1568-1581.

Sorkin A & von Zastrow M. (2009). Endocytosis and signalling: intertwining molecular networks. *Nature reviews Molecular cell biology* 10, 609-622.

Sun Y, Chen M, Lowentritt BH, Van Zijl PS, Koch KR, Keay S, Simard JM & Chai TC. (2007). EGF and HB-EGF modulate inward potassium current in human bladder urothelial cells from normal and interstitial cystitis patients. *American Journal of Physiology-Cell Physiology* 292, C106-C114.

Sunder-Plassmann R, Lialios F, Madsen M, Koyasu S & Reinherz EL. (1997). Functional analysis of immunoreceptor tyrosinebased activation motif (ITAM)-mediated signal transduction: the two YxxL segments within a single CD3ζITAM are functionally distinct. *European journal of immunology* 27, 2001-2009.

Tong Y, Brandt GS, Li M, Shapovalov G, Slimko E, Karschin A, Dougherty DA & Lester HA. (2001). Tyrosine decaging leads to substantial membrane trafficking during modulation of an inward rectifier potassium channel. *The Journal of general physiology* 117, 103-118.

Vaidyanathan R, Vega AL, Song C, Zhou Q, Tan B, Berger S, Makielski JC & Eckhardt LL. (2013). The Interaction of Caveolin 3 Protein with the Potassium Inward Rectifier Channel Kir2. 1 PHYSIOLOGY AND PATHOLOGY RELATED TO LONG QT SYNDROME 9 (LQT9). *Journal of Biological Chemistry* 288, 17472-17480.

Varkevisser R, Houtman MJ, Waasdorp M, Man JC, Heukers R, Takanari H, Tieland RG, en Henegouwen PMvB, Vos MA & van der Heyden MA. (2013). Inhibiting the clathrin-mediated endocytosis pathway rescues KIR2. 1 downregulation by pentamidine. *Pflügers Archiv-European Journal of Physiology* 465, 247-259.

Wischmeyer E, Döring F & Karschin A. (1998). Acute suppression of inwardly rectifying Kir2. 1 channels by direct tyrosine kinase phosphorylation. *Journal of Biological Chemistry* 273, 34063-34068.

Xu X, Kanda VA, Choi E, Panaghie G, Roepke TK, Gaeta SA, Christini DJ, Lerner DJ & Abbott GW. (2009). MinK-dependent internalization of the IKs potassium channel. *Cardiovascular research*.

Zeng W-Z, Babich V, Ortega B, Quigley R, White SJ, Welling PA & Huang C-L. (2002). Evidence for endocytosis of ROMK potassium channel via clathrin-coated vesicles. *American Journal of Physiology-Renal Physiology* 283, F630-F639.

Zhao Z, Liu B, Zhang G, Jia Z, Jia Q, Geng X & Zhang H. (2008). Molecular basis for genistein-induced inhibition of Kir2. 3 currents. *Pflügers Archiv-European Journal of Physiology* 456, 413-423.

Acknowledgement

First and foremost, I would like to express my deepest gratitude to Prof. Jürgen Daut for giving me the opportunity, his excellent guidance, caring, patience, practical support and providing me with excellent platform for my PhD studies. He has been a tremendous mentor for me. I would like to thank my second supervisor Dr. Vijay Renigunta for his dedicated mentorship, the intellectual, enthusiasm and immense knowledge in all the time of research and writing this thesis.

I would like to thank Dr. Thomas Fischer and Dr. Marylou Zuzarte for their kind support in the imaging experiments and Dr. Günther Schlichthörl for the help regarding the electrophysiology measurements.

I would also like to thank Dr. Wiebke Milani, Dr. Regina Preisig-Müller. Stefan Kling, Kristin Koschinsky, Julia Schiekel, Katrin Grothus, Xinle Zou, Doris Wagner, Kirsten Ramlow, Andrea Schubert for the friendly atmosphere, the willingness to help and all the fun in the whole AG Daut lab.

My sincere thanks also go to secretary, Susanne Bamerny, for reducing our burdens in dealing with administrative stuff.

I am also indebted to my friend, Yunbo Yang, who squeezes time from his busy schedule to help me handle my personal stuff in the life.

A special thanks to my family. I am very grateful for their continuous supporting me spiritually throughout my life.

Verzeichnis der akademischen Lehrer

Meine akademischen Lehrer waren

in Marburg:

Daut, Renigunta.

in Beijing:

Cai, Guo, Gao, Hou, Jiang, Li, Wang, Xiao.

Ehrenwörtliche Erklärung

Ich erkläre ehrenwörtlich, dass ich die dem Fachbereich Medizin Marburg zur Promotionsprüfung eingereichte Arbeit mit dem Titel “Endocytosis of the potassium channel Kir2.1” im Institut für Physiologie und Pathophysiologie der Philipps-Universität Marburg unter Leitung von Prof. Dr. Dr. Jürgen Daut ohne sonstige Hilfe selbst durchgeführt und bei der Abfassung der Arbeit keine anderen als die in der Dissertation aufgeführten Hilfsmittel benutzt habe. Ich habe bisher an keinem in oder ausländischen Medizinischen Fachbereich ein Gesuch um Zulassung zur Promotion eingereicht, noch die vorliegende oder eine andere Arbeit als Dissertation vorgelegt.

Marburg, den 15. 12. 2014

(Wei Tu)